

Risk-Sensitive Learning in Population Games under Extreme Events: Bifurcations and Chaotic Dynamics

Konstantinos Metaxas ^{*}, Themistoklis P. Sapsis [†]
 Department of Mechanical Engineering,
 Massachusetts Institute of Technology,
 77 Massachusetts Ave., Cambridge, MA 02139

Abstract

Inspired by nonequilibrium phenomena in game dynamics and behavioral evidence on the impact of extreme events on decision making, we investigate the nonlinear dynamics of a discrete-time multiagent learning rule in population congestion games under extreme events affecting one of the actions. The population state, following a risk-sensitive variant of the Multiplicative Weights Update (MWU), is coupled with a belief variable capturing the agents perceived risk and updated through an adaptive expectation rule. We perform a two-parameter bifurcation analysis with respect to the agents controlled parameters, identifying regions of qualitatively distinct behavior. Equilibria are studied first from both game-theoretic and dynamical perspectives. The resulting two-dimensional system exhibits complex behavior, including multi-stability among fixed points, invariant curves, periodic and chaotic attractors. Despite this complexity, the attractors can be grouped into distinct families, while the Cesàro averages of the trajectories are shown to converge to the stationary equilibrium. The incorporation of risk associated with the extreme event leads to new dynamical phenomena: attracting invariant curves arise and give rise to phase-locking Arnold tongues, within which the dynamics is qualitatively similar. In this setting, codimension-two resonances are identified as organizing centers, both within individual tongues and along the bifurcation curves associated with the fixed-point family. Chaotic attractors emerge and are destroyed through Feigenbaum cascades and forward or reverse boundary crises, with interior and merging crises also observed, along with transient chaos and narrow periodic windows. For each qualitatively distinct region, representative phase portraits and the associated basins of attraction are examined.

Keywords: Bifurcations, Nonlinear dynamics, Chaos, Game dynamics, Population games, Extreme events

1 Introduction

Congestion games constitute one of the most fundamental and widely studied families of games in game theory [67, 54]. They are typically used as models in settings where agents jointly utilize a set of shared resources, with the cost of each resource determined by its level of congestion. Mirroring biological adaptation, multiagent reinforcement learning suggests that agents utilize the outcomes of their past actions to adapt to the game and select their subsequent actions [14, 69]. In this context, the agents behavior in congestion games can be viewed as aiming to minimize a common potential function [54, 10]. In the limit of a very large population of interacting agents, the learning process is studied at the population level and the game is referred to as population or nonatomic. Several results establish convergence to the Nash equilibrium in both continuous-time and discrete-time settings, provided, in the latter case, that the learning rate is sufficiently small [69, 58, 54, 43].

The behavior of the system as learning rates deviate from this threshold, or more broadly the question of the potential complexity of agents behavior in games, has attracted significant attention. The seminal work of [71] has shown that even in simple zero-sum two-player games, such as rock-paper-scissors, the continuous-time replicator dynamics of evolutionary game theory [69, 39, 1, 13, 31, 30] can exhibit Hamiltonian chaos, while Hamiltonian and Poisson structures of zero-sum replicator dynamics have also been further investigated in [34]. Several subsequent works have further investigated chaotic dynamics in continuous-time learning [72, 70], while chaos has also been established in fields at the intersection of evolution and game theory [56, 16, 86, 44, 61]. In fact, the dynamics of any complex system can be reproduced by agents learning a suitable matrix game under replicator dynamics [3]. Important works on stochastic variants of replicator dynamics in zero-sum games [27], and more generally on stochastic effects in evolutionary game dynamics [46], have also been carried out. Related nonlinear evolutionary-game models have investigated the effects of delayed payoffs, memory, mutation feedback, density dependence, and finite-population

^{*}metaxas@mit.edu

[†]sapsis@mit.edu

or spatial effects on the stability and complexity of the dynamics [87, 11, 82, 81, 35]. Applications of evolutionary game dynamics include social dilemmas, cooperation, public-goods interactions, and resource-management problems [53, 49, 28, 26, 47, 50, 84, 85].

In discrete time, where players make decisions in a round-by-round manner, the Multiplicative Weights Update (MWU) [29] and its generalization Follow-the-Regularized-Leader can be viewed as discrete-time analogues of the corresponding continuous-time Hamiltonian dynamics which are recurrent [7, 12]. However, when agents learn using these rules in zero-sum games, the resulting dynamics can exhibit Lyapunov chaos [52, 6, 18, 19]. Complex behavior has also been shown to arise in nonatomic two-strategy congestion games with agents employing MWU [21, 20, 58, 8], and persists in heterogeneous settings [10], where agents have different learning rates [36] or when learning rates are adaptively updated [80]. Related studies of nonlinear evolutionary-game dynamics have also emphasized the role of adaptive update rules, network structure, attractors, and basins of attraction [37, 74]. In more complex games with two or more players, chaos has been observed when agents utilize the Experience-Weighted Attraction rule of behavioral game theory, although memory loss, acting as a perturbation to standard MWU dynamics, can lead to more predictable behavior [32, 68, 9, 60]. Chaotic behavior has also been observed in auctions [17] and in dynamics induced by fictitious play learning rules [73, 78], gradient descent-ascent algorithms [5], as well as in discretized replicator dynamics [55, 59, 79]. Beyond learning and evolutionary dynamics, nonlinear strategic adjustment models in economic games, including duopoly, triopoly, oligopoly and Cournot-type games, have been known to exhibit complex bifurcation structures and chaos [65, 42, 76, 51, 2, 83].

According to behavioral decision theory, low-probability, high-impact outcomes may affect individuals responses by shaping their perceived risk, memory, and subsequent decision making [41, 77]. Thus, an extreme event not only has a material consequence but also adaptively affects an individual's perception and memory. From the perspective of decisions from description and experience, the influence of extreme events on decision making is closely tied to memory and learning from realized outcomes [63, 38]. In the context of learning in games, extreme events become particularly relevant in real-world settings where agents adapt their strategies under uncertainty, and the learning process becomes coupled with their internal perception of risk [14, 15]. In fact, consistent with experience-based decision making, the behavioral impact of extreme events extends to the agents adaptive learning process, making them an important endogenous factor [62]. Despite extensive research on complex dynamics induced by learning in games and behavioral game theory, the effect of rare, high-impact events on population dynamics has received limited direct attention. This raises the question of what new bifurcations, attractors and dynamical phenomena may arise from the behavioral impact of such events.

Motivated by the above discussion, the present work investigates the nonlinear dynamics and bifurcations induced by learning in the presence of relatively extreme events in the simplest class of population games, namely two-action congestion games. It is assumed that an extreme event affects the first resource, which agents perceive through a shared signal. To illustrate the complexity of the learning dynamics, it suffices to consider a simple linear dependence of this signal on the population state. Consistent with observations from human behavior, the population state is augmented by a belief variable capturing the agents perception or memory of the risk associated with the first action. This variable is updated through a standard discrete-time adaptive expectation rule [40]. Each agent follows a risk-sensitive variant of the discrete-time reinforcement learning MWU algorithm, in which the belief about the risk enters the cost, making the system two dimensional.

We first study the equilibria of the system from both dynamical and game-theoretic perspectives. Similar to traditional MWU dynamics, the system admits two trivial equilibria corresponding to the boundary cases of the population state. The equilibrium associated with the full-population state is always a saddle, while the one corresponding to the zero-population state is stable only in parameter regimes associated with non-extreme events. In this case, the dynamics is trivial, since the equilibrium is globally attracting and also game-theoretically stationary. When this equilibrium is a saddle, a third interior equilibrium exists, which is always stationary. Using numerical continuation techniques [25, 22], we compute bifurcation curves in a two-dimensional parameter space defined by the key parameters controlled by the agents, namely the learning rate and the belief adjustment rate, thereby identifying regions of qualitatively distinct behavior. The system under study exhibits complex behavior, including chaotic attractors emerging through Feigenbaum cascades, crisis bifurcations [75, 33, 57, 48] leading to the destruction, creation, or expansion of strange attractors, stable invariant curves, phase-locked periodic orbits, codimension-two resonances, and multistability among these attractors. In addition to detailed bifurcation diagrams, we analyze representative cases of multistability through basins of attraction and phase portraits. We also calculate the associated basin entropy (S_b) and boundary basin entropy (S_{bb}), which quantify the unpredictability and mixing properties of the basins [23, 66, 24]. In this way, fractal structure of the basin boundaries is inferred. A case of fully mixed ($S_b = S_{bb}$) non-Wada basins is also identified. Transient chaos and narrow periodic windows in parameter space are observed in the presence of chaotic saddles. Despite the complexity of the system, the attractors form well-defined families and exhibit qualitatively similar dynamical phenomena. In particular, the codimension-two structure of the periodic families is consistent across different families, while the basins of attraction are typically highly intermingled. Finally, the Cesàro time averages of the orbits are shown to converge to the stationary equilibrium, even in cases exhibiting complex and chaotic dynamics.

Note that the two-dimensional nature of the system allows for several phenomena that are absent from the MWU variants studied so far. Indicative examples include Neimark–Sacker bifurcations, Arnold tongues, and codimension-two resonances, which have not been identified in traditional MWU dynamics for population games, even in the heterogeneous setting [10]. Moreover, the stationary interior equilibrium may be stable without being the global attractor, coexisting with both chaotic and periodic attractors. Finally, for large values of the learning rate, the system exhibits predictable periodic behavior, in stark contrast to the one-dimensional MWU case.

This paper is organized as follows. In Section 2, we first briefly discuss traditional learning in congestion games under MWU, and then introduce and study the fundamental properties of the system induced by the risk-sensitive learning rule. Technical details for this Section are provided in Appendix A. In Section 3, a detailed bifurcation analysis of the system is conducted, qualitatively distinct attractor families are identified, and the complex and chaotic dynamics of the system are discussed in depth. Finally, Section 4 concludes the article.

2 Model and fundamental properties

In this Section, we introduce and discuss the fundamental properties of the risk-sensitive variant of the Multiplicative Weights Update algorithm (MWU), whose nonlinear dynamics we study in detail in Section 3. We first briefly discuss the setting of learning congestion games under the standard multi-agent reinforcement learning algorithm MWU [58, 4].

2.1 Learning congestion games with MWU

We consider a two-strategy non-atomic congestion game, i.e., a game with a continuum of agents [6, 19]. Let $x_n \in [0, 1]$ denote the fraction of agents choosing action 1 at time n , so that the corresponding flows on actions 1 and 2 are Nx_n and $N(1 - x_n)$, respectively, where $N > 0$ is the total population mass. The realized stage costs are given by

$$c_1 = N\gamma x_n, \quad c_2 = Nb(1 - x_n), \quad (1)$$

where the parameters $\gamma, b > 0$ are the coefficients of proportionality and satisfy $\gamma + b = 1$ [9]. When the agents learn according to MWU, their choices evolve as

$$\begin{aligned} x_{n+1} &= \frac{x_n \exp(-\lambda c_1(x_n))}{x_n \exp(-\lambda c_1(x_n)) + (1 - x_n) \exp(-\lambda c_2(1 - x_n))} \\ &= \frac{x_n}{x_n + (1 - x_n) \exp(a(x_n - b))}, \end{aligned} \quad (2)$$

where $\lambda = -\log(1 - \epsilon)$ describes the intensity of choice, $a = N\lambda$ denotes the population intensity of choice, and $\epsilon \in (0, 1)$ is the common learning rate.

The dynamical system (2) has the boundary fixed points 0 and 1, as well as the interior fixed point b . The boundary fixed points are always repelling, while the interior fixed point is globally attracting if $a \leq \frac{2}{b(1-b)}$ [21]. If this condition does not hold, then complex behavior may arise, including periodic orbits and chaos for sufficiently large values of a [21]. However, the Cesàro mean of any orbit always converges to b [21]—cf. the analogous result described in Proposition 1 for the risk-sensitive case we will be considering.

From a game-theoretic perspective a *Nash equilibrium* is a mixed strategy determined by a fraction x^N , with the first action played with probability x^N and the second with probability $1 - x^N$, such that no agent can improve their payoff by unilaterally deviating to another strategy. Recalling (1), one can immediately see that the interior equilibrium b is always a Nash equilibrium.

The intricate dynamics of this simple and fundamental model in multi-agent reinforcement learning have led to the investigation of several variants of the standard MWU learning rule [20, 58, 8, 10, 9, 80], including heterogeneous learning rates [10, 36] and adaptively updated learning rates [80]. These works indicate that complex behavior persists under several extensions, while discounting through memory loss may, under certain conditions, lead to the avoidance of chaos [9].

Despite the plethora of studied extensions of MWU, as also discussed in Section 1, the complexity of the dynamics when agents incorporate perceived risk and memory, associated with the costs of actions, stemming from a low-probability extreme event has not received much direct attention. This is particularly relevant because extreme events are known to affect the decision-making and adaptation process by coupling it with risk perception [14, 15, 63, 38]. Moreover, from a dynamical-systems perspective, the consideration of such a model offers the possibility of new phenomena that are absent from the existing literature on the dynamics of MWU. The purpose of this paper is to offer a first step towards addressing this gap. To this end, in the next subsections of Section 2, we introduce and discuss the risk-sensitive model whose dynamics and bifurcations we study in detail in Section 3.

2.2 Risk-sensitive MWU variant

In this subsection, we introduce the risk-sensitive variant considered in this paper. We consider a non-atomic congestion game as in Section 2.1 and use the same notation. However, we now suppose that an extreme event affects action 1, i.e., the realized stage costs are given by

$$C_1 = N(\gamma x_n + MU_n), \quad C_2 = Nb(1 - x_n), \quad (3)$$

where $U_n \in \{0, 1\}$ is a random variable corresponding to an extreme (and, thus, low-probability) event affecting action 1 and $M > 1$ corresponds to its intensity. The parameters $\gamma, b > 0$ are as in Section 2.1. We suppose that the agents, instead of knowing explicitly the law of U_n , perceive the occurrence of such an event through a (shared) signal generated by the environment. To illustrate the complexity induced in the learning dynamics by this mechanism, it is sufficient to consider the simple model that represents the probability (risk) for an extreme event

$$p(x_n) = p_0 + p_1 x_n, \quad (4)$$

where $p_0, p_1 \geq 0$ (of the order of 10^{-3} or less). Here p_0 represents the exogenous baseline risk of action 1, while the term $p_1 x_n$ captures the endogenous dependence of the perceived risk on the use of that action. Thus, $p_0 + p_1 x_n$ is interpreted as the perceived risk signal for extreme event, associated with action 1 at time n .

To model risk perception and belief, we introduce a homogeneous belief (or memory) variable $q_n \in [0, 1]$, representing the agents common internal assessment of the extreme-event risk at time n . Learning and remembering the perceived risk of an action and making decisions based on it is a common modeling approach in decision-making from experience motivated by the human behavior [64, 38]. Outside of the connection to extreme events, the q state can be thought of as representing an internal variable that is recursively updated and that, together with the observable state x , determines the players choices, a modeling approach commonly used in learning and behavioral dynamics [14].

The evolution of this belief is assumed to follow the standard adaptive rule

$$q_{n+1} = (1 - k)q_n + k(p_0 + p_1 x_n), \quad k \in (0, 1], \quad (5)$$

where the next iterate belief is a convex combination of the current internal assessment and the perceived risk signal. The parameter k governs the speed of belief adjustment. Equivalently, it can be seen as the standard discrete-time form of adaptive expectations or exponential smoothing. Rather than reacting directly to the instantaneous signal $p_0 + p_1 x_n$, agents evaluate the extreme-event component of action 1 using q_n as their current perceived event probability and amplify the intensity M by a factor $1/(1 - \alpha)$, $\alpha \in (0, 1)$. This constitutes essentially a simplified version of the Conditional Value-at-Risk measure at confidence level α ; more details on this matter are given in Appendix A.2. Accordingly, the perceived cost of action 1 is

$$\tilde{c}_1(x_n, q_n) = N(\gamma x_n + cq_n), \quad (6)$$

where $c = M/(1 - \alpha)$ is the effective intensity. The perceived cost of action 2 is

$$\tilde{c}_2(x_n) = Nb(1 - x_n). \quad (7)$$

Under the normalization $\gamma + b = 1$, the perceived relative cost becomes

$$\Delta(x_n, q_n) = \tilde{c}_1(x_n, q_n) - \tilde{c}_2(x_n) = N(x_n - b + cq_n). \quad (8)$$

Let $\epsilon \in (0, 1)$ denote the common learning rate and set $\lambda = -\log(1 - \epsilon)$, $a = N\lambda$. Then, following the same computations as in the derivation of (2), the risk-sensitive Multiplicative Weights dynamics is given by

$$\begin{aligned} x_{n+1} &= \frac{x_n}{x_n + (1 - x_n) \exp(a(x_n - b + cq_n))} \\ q_{n+1} &= (1 - k)q_n + k(p_0 + p_1 x_n). \end{aligned} \quad (9)$$

We refer to the previous dynamics as *risk-sensitive*, due to the coupling of the population state x with the perceived risk modeled by q , resulting from the evaluation of risk in the cost of the first resource. In the following sections we study the complex dynamics induced by the learning rule defining the system (9), which we denote by $(x, q) \mapsto f(x, q) = (f_1(x, q), f_2(x, q))$.

2.3 Equilibria and fundamental properties

In this subsection we determine the system's equilibria (both dynamically and game-theoretically) and discuss the fundamental properties of system (9), including the convergence of the time averages of every orbit to the stationary equilibrium, a property similar to that of the traditional MWU discussed in Section 2.1.

The dynamical system (9) has the trivial fixed points $(0, p_0)$, $(1, p_0 + p_1)$. The first equilibrium is stable if and only if $b < cp_0$, while the second one is always a saddle, as it is unstable in the x -direction. If $b_0 < cp_0$, then the dynamics is trivial, since the fixed point $(0, p_0)$ attracts all orbits, as shown in Lemma 2 in the Appendix A.1. If $b > cp_0$ the system has the interior equilibrium (x^*, q^*) , where

$$x^* = \frac{b - cp_0}{1 + cp_1}, \quad q^* = \frac{p_0 + p_1 b}{1 + cp_1}, \quad c = \frac{M}{1 - \alpha}. \quad (10)$$

In that case, regarding the boundary equilibria, we also have the following property (shown in Lemma 1): for every orbit there is a $\delta > 0$ such that $x_n \in (\delta, 1 - \delta)$ for all n . The more interesting questions about the stability and the related bifurcations of this equilibrium are studied in detail in the next sections.

In terms of game-theoretic equilibria, a stationary equilibrium with consistent beliefs is a pair (x^N, q^N) with x^N a Nash equilibrium (cf. Section 2.1) and $q^N = p_0 + p_1 x^N$. Stationary equilibria form a subset of the fixed points of the system. It is easy to check that $(1, p_0 + p_1)$ is never a stationary equilibrium. If $b < cp_0$, i.e., the $(0, p_0)$ equilibrium is stable and the interior equilibrium does not exist, then $(0, p_0)$ is also a stationary equilibrium. Thus, in this trivial case, where the extreme event is sufficiently strong and relatively likely to occur, all trajectories converge to the Nash equilibrium of the system. In the more interesting case of $b > cp_0$, the trivial equilibrium $(0, p_0)$ is not a stationary equilibrium of the system, while the interior one, (x^*, q^*) , satisfies both the condition of Nash equilibrium $\Delta(x^*, q^*) = 0$ and $q^* = p_0 + p_1 x^*$, and is therefore the only stationary equilibrium.

As noted in the previous Section, system (9) is closely related to the one obtained when agents evaluate the perceived risk using the CVaR $_\alpha$ risk measure. The dynamics of the two systems are also closely related. These connections are discussed in Appendix A.2.

We now prove the convergence of time-averages of the trajectories of the system (9) to the stationary equilibrium, even when the induced dynamics is complex, as is shown in the next sections. This result can be viewed as an analogue of the corresponding result for traditional MWU.

Proposition 1. *If $x_0 \in (0, 1)$, then we have the following convergences*

$$\lim_{n \rightarrow \infty} \frac{1}{n+1} \sum_{i=0}^n x_i = x^*, \quad \lim_{n \rightarrow \infty} \frac{1}{n+1} \sum_{i=0}^n q_i = q^*. \quad (11)$$

Proof. The case $b \leq cp_0$ is trivial, as the stationary equilibrium is a global attractor of the system. Suppose that $b > cp_0$. Inductively we have that

$$x_{n+1} = \frac{x_0}{x_0 + (1 - x_0) \exp(a \sum_{i=0}^n (x_i - b_i))}, \quad b_i = b - cq_i.$$

From Lemma 1, there exists a $\delta \in (0, 1)$ such that $\delta < x_n < 1 - \delta$ for all n . Thus,

$$\frac{x_0}{1 - \delta} < x_0 + (1 - x_0) \exp\left(a \sum_{i=0}^n (x_i - b_i)\right) < \frac{x_0}{\delta}$$

and so

$$\delta^2 < \frac{\delta^2}{1 - x_0} < \frac{x_0 \delta}{1 - \delta} < \exp\left(a \sum_{i=0}^n (x_i - b_i)\right) < \frac{x_0(1 - \delta)}{\delta(1 - x_0)} < \frac{1}{\delta}.$$

As a result,

$$\lim_{n \rightarrow \infty} \frac{1}{n+1} \sum_{i=0}^n (x_i + cq_i) = b.$$

Now let

$$A_n = \frac{1}{n+1} \sum_{i=0}^n x_i, \quad B_n = \frac{1}{n+1} \sum_{i=0}^n q_i.$$

From (5) we have that

$$\frac{q_{n+1} - q_0}{n+1} = k(p_0 + p_1 A_n - B_n),$$

and thus

$$\lim_{n \rightarrow \infty} (1 + cp_1) A_n + p_0 - \frac{q_{n+1} - q_0}{k(n+1)} = b.$$

This implies, since q_n is bounded, that

$$A_n = \frac{1}{n+1} \sum_{i=0}^n x_i \xrightarrow{n \rightarrow \infty} x^*.$$

The convergence of the time average of q_n follows. □

The previous property suggests immediately one further regularity result: if μ is a probability measure on $[0, 1] \times [0, p_0 + p_1]$ invariant under f and such that $\mu(\{0, 1\} \times [0, p_0 + p_1]) = 0$, then Birkhoff’s ergodic theorem implies that

$$\int (x, q) d\mu = (x^*, q^*).$$

3 Bifurcation analysis and chaotic dynamics

Table 1: Primary attractor families discussed in the text. The bifurcation curves refer to those shown in Figs. 1, 9, and 13. The descriptor “t” denotes an attracting invariant curve. When the original attractor is periodic or a fixed point, the last column indicates its period. Saddle-node bifurcations are denoted by SN, and Neimark–Sacker bifurcations by NS. All families are destroyed through the corresponding boundary crisis, except for family VII.

Family	Birth	Original Family’s Period
I	SN1	3
II	–	1
II-t	NS ₂ ¹ or NS ₂ ² or inverse boundary crisis	–
III	SN3	9
IV	SN4	4
V	SN5	7
II-i	SN _{2-i} or NS ₂₋₅	<i>i</i>
VI	SN _{6-j} or NS _{6-j} ¹	<i>j</i>
VII	SN ₇₋₅	5
I-IV-V	Interior or inverse boundary crisis	–
I/II	Interior crisis	–
I/II/IV	Interior crisis	–

¹ The SN_{6-j} curves are denoted by SN_{*j*} in Figs. 9 and 13 for simplicity, while the labels NS_{6-j} have been omitted from the corresponding curves in the figures for clarity.

In this Section, we study in detail the nonlinear dynamics and the associated bifurcations of the system described by (9). The analysis is based on numerical techniques, since analytical tools (such as the center manifold theorem or normal form theory) are only valid locally around the corresponding equilibrium or cycle and would not reveal the global dynamics. We consider the parameters of the extreme event p_0, p_1, M and the parameters b, α fixed, and study how the parameters controlled by the agents, namely a and k , affect the learning dynamics. We assume, as stated that $b > cp_0$, which induces non-trivial dynamics, as otherwise the $(0, p_0)$ equilibrium is the global attractor of the system. In the following, let $p_0 = 10^{-5}$, $p_1 = 10^{-3}$, $M = 15$, $\alpha = 0.97$, $b = 0.3$. Different choices of these parameters would result in quantitative differences, retaining the qualitative picture discussed next. In the last subsection we elaborate briefly on this matter. The bifurcation curves have been computed via continuation techniques following [25, 22].

Despite the regularity results discussed in the previous Section, the dynamics is fairly complex and for this reason we divide the (a, k) parameter space into distinct regions, on which we focus. Although most bifurcations are contained in, and can be described within, the first two regions, we also study a third region to highlight differences in the stability, coexistence and merging of the attractors depending on the order of the occurring bifurcations. Importantly, we show in the following that, despite the complexity of the underlying dynamics, the attractors are organized into specific families, and the mechanisms governing their birth and destruction follow similar qualitative patterns. Table 1 summarizes the main attractor families of the system, with regular numerals replacing the Latin ones in the respective figures for the sake of clarity. In what follows saddle-node bifurcations are denoted by SN, period-doubling bifurcations by PD, and Neimark–Sacker bifurcations by NS.

3.1 Dynamics within the first region

We begin with the region in Fig. 1, containing the primary bifurcation curves of the periodic orbits. To illustrate the qualitatively distinct attractors, suppose we fix $k = 0.865$ and gradually increase a . Fig. 2 depicts the resulting bifurcations as a varies. At low values of the parameter a the Nash equilibrium is the unique attractor of the system. As the learning rate and, thus a , increases, a stable period-three cycle (family I, c.f. Table 1) emerges corresponding to the crossing of the SN₁ curve of Fig. 1. Its basin of attraction is shown in Fig. 3 (a). This cycle undergoes a cascade of period-doubling bifurcations, the first two of which correspond to the PD₁¹, PD₁² curves of Fig. 1. As SN₃

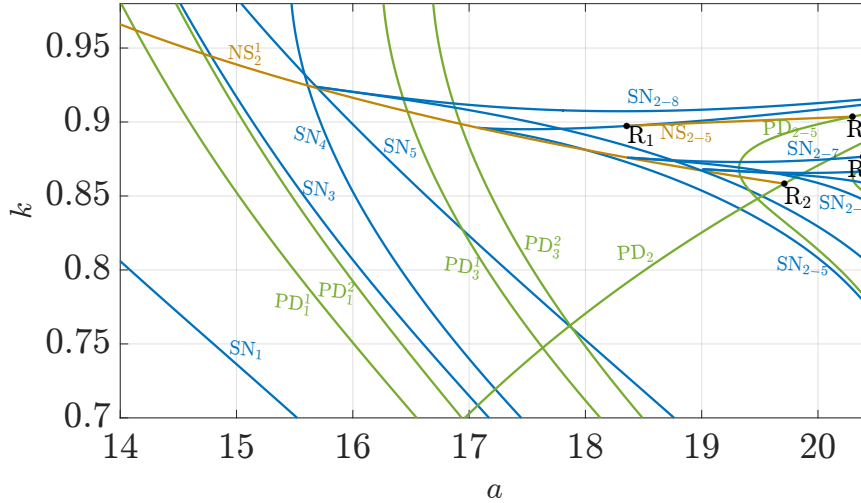


Figure 1: Bifurcation curves in the first region. Saddle-node bifurcations are denoted by SN, period-doubling bifurcations by PD, and Neimark-Sacker bifurcations by NS. Bifurcation curves of the same type share the same color. The index of each curve refers to the attractor family of Table 1. The superscript in the PD and NS curves refers to their order in the respective family. The labels R_1 correspond to 1 : 1 strong resonances, while the labels R_2 to 1 : 2 strong resonances.

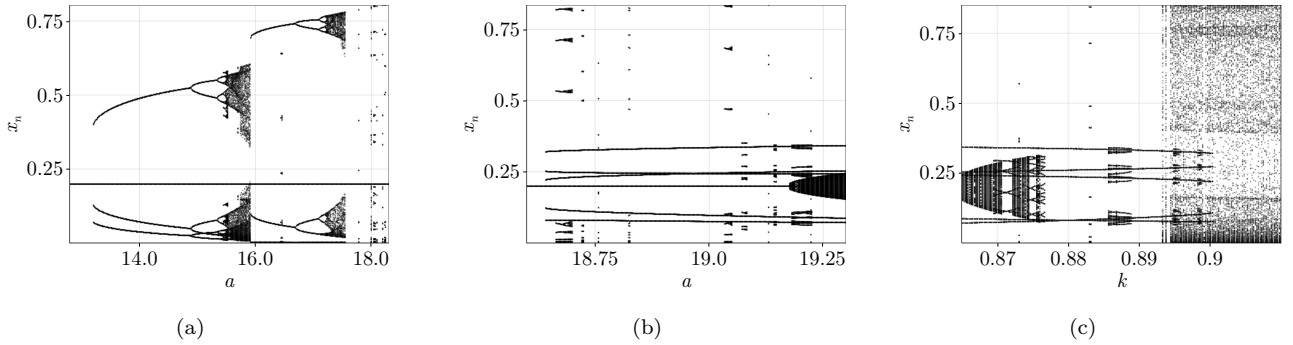


Figure 2: (a), (b) The various emerging attractors as $k = 0.865$ is held fixed and a is gradually increased. Each attractor birth corresponds to the crossing of a bifurcation curve of Fig. 1 or to a crisis. (c) Attractors as $a = 19.3$ is fixed and k varies.

is crossed a period 9 cycle is born (family III), which in turn experiences a Feigenbaum route to chaos. The basins of attraction and the phase space, when both strange attractors and the stable equilibrium are present, are illustrated in Fig. 3(b) and Fig. 4(a), respectively. It is worth noting that the basin boundaries have become intermingled and are of fractal type. A natural way to quantify this observation is via determining the basin entropy (S_b) and boundary basin entropy S_{bb} [23, 66, 24], reported in Table 2. The former quantifies the overall unpredictability of the system in terms of which attractor an initial condition converges to, while the latter measures the intensity of mixing at the boundary. Since S_{bb} satisfies the fractality criterion proposed in [66, 24], the basin boundaries have indeed fractal structure, in contrast to the boundaries in Fig. 3 (a).

Varying further the parameters, the chaotic attractor originating from the nine-period cycle experiences a basin crisis bifurcation, resulting in its conversion to a chaotic saddle. A part of its saddle set collides with the basin of the chaotic attractor of family I, leading to its expansion, as shown in Fig. 4(b) and Fig. 3(c) with the associated basin and boundary basin entropies reported in Table 2. We keep referring to this expanded family as I.

Crossing SN_4 of Fig. 1 results in the birth of stable four-period cycle (family IV), while almost simultaneously another boundary crisis bifurcation involving the chaotic attractor of family II results in its transformation into a chaotic saddle (c.f. Fig. 2(a)). A stable period-seven cycle (family V) appears at SN_5 , coexisting with the family II and family IV and which within a very narrow parameter region, period-doubles to chaos and in turn transforms to a chaotic saddle through a boundary crisis. Similar to family I, family IV undergoes a similar pattern of Feigenbaum cascades, expansion through an interior crisis and eventual destruction through a boundary crisis. The phase space and the basin of attraction before the destruction of the IV family chaotic attractor are shown in Fig. 4(c) and Fig. 5(a). Although the families I, IV and V have lost their stability, they affect the dynamics of the system through the infinitely many unstable periodic orbits living inside the chaotic saddle. In fact, the chaotic saddles of these

Table 2: Basin and boundary basin entropy. According to the fractal criterion proposed in [66, 24], the basin boundary has fractal structure if $S_{bb} > 0.439$.

Figure	S_b	S_{bb}	Figure	S_b	S_{bb}
Fig. 3(a)	0.110	0.350	Fig. 7(a)	0.790	0.810
Fig. 3(b)	0.386	0.572	Fig. 7(b)	0.589	0.611
Fig. 3(c)	0.198	0.540	Fig. 7(c)	0.879	0.898
Fig. 5(a)	0.220	0.563	Fig. 7(d)	0.620	0.639
Fig. 5(b)	0.490	0.577	Fig. 11(b)	0.731	0.731
Fig. 5(c)	0.790	0.826	Fig. 12(a)	0.012	0.423
Fig. 5(d)	0.650	0.635	Fig. 12(b)	0.001	0.220
Fig. 5(e)	0.795	0.826	Fig. 12(c)	0.006	0.556
Fig. 5(f)	0.588	0.620	Fig. 12(d)	0.096	0.241

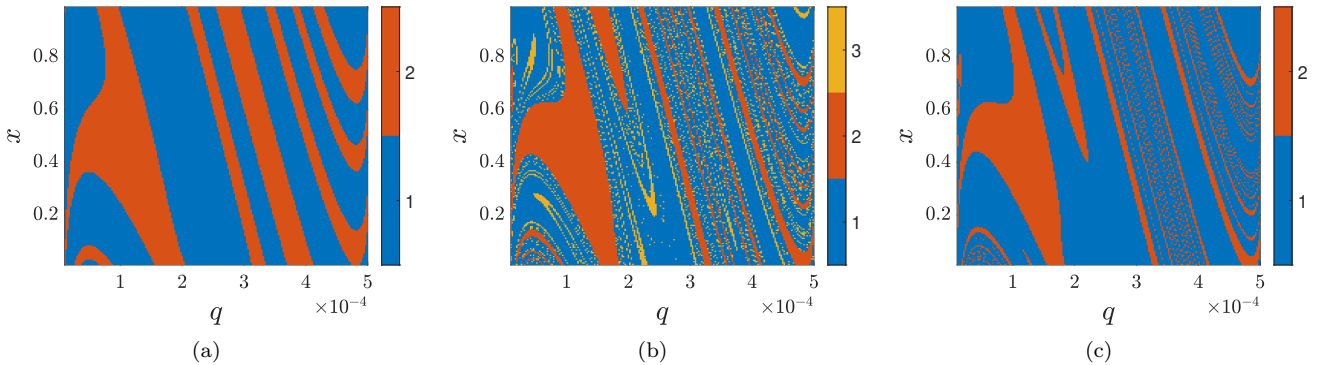


Figure 3: Basins of attraction of the coexisting attractors with $k = 0.865$ fixed, corresponding to Fig. 2(a). The numerical labels 1, 2, ... correspond to the Roman-numeral family indices I, II, ..., defined in Table 1. (a) $a = 14.02$: The period three orbit and the equilibrium coexist. (b) $a = 15.5225$: The chaotic attractor of family I, the equilibrium and the chaotic attractor of family III coexist. (c) $a = 15.8$: The chaotic attractor of family I and the equilibrium coexist. Note the intermingling of the basins in (b) and (c).

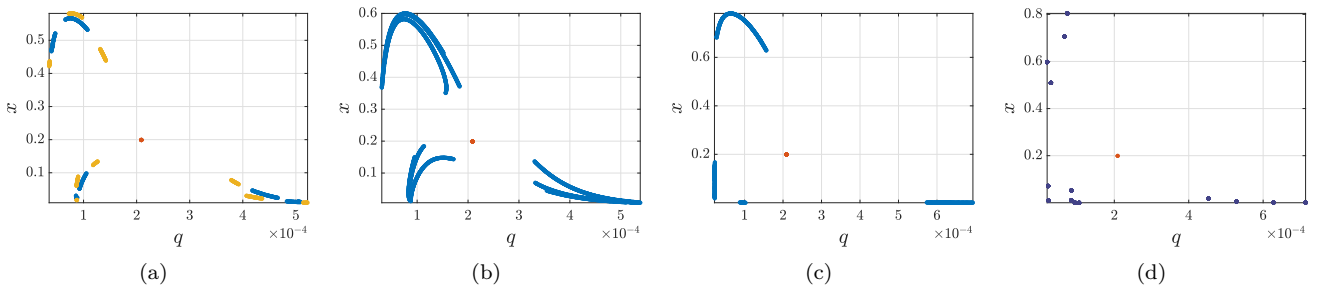


Figure 4: Coexisting attractors in the phase space. (a) $a = 15.5225$: The chaotic attractor of family I, the equilibrium and the chaotic attractor of family III coexist. (b) $a = 15.8$: The chaotic attractor of family I and the equilibrium coexist. (c) $a = 17.54$: The merged chaotic attractor I-IV-V and the equilibrium coexist. (d) $a = 18.245$: A high-period orbit of the I-IV-V family coexists with the stable equilibrium. In all cases $k = 0.865$ fixed.

families become connected, while the embedded unstable periodic orbits lead to the emergence of high-period stable periodic orbits—whose family we call, abusing notation, I-IV-V—within small regions of the parameter space, which in turn undergo period-doubling bifurcations before they get destroyed via boundary crises. Typical examples are shown in Fig. 2(a), where, within narrow regions of the parameter space, high-period cycles follow the described pattern. It is worth noting that the basins of the I-IV-V-type attractors are highly intermingled—cf. Fig. 5(b) and Table 2. The phase space, when a high-period orbit of the I-IV-V family coexists with the stable equilibrium is shown in Fig. 4(d). Another manifestation of the chaotic saddle is that, despite the stationary equilibrium being the sole attractor after the boundary crisis, the system is transiently chaotic with orbits spending large amount of time near the chaotic saddle, and thus having positive finite Lyapunov exponent, as illustrated in Fig. 5 (c). We note that none of the I, III, IV and V periodic attractors exhibit any codimension-2 bifurcations.

At NS_2^1 (c.f. Fig. 1) the stable equilibrium loses stability and a stable invariant curve emerges, whose family in Table 1 is referred to as II-t (essentially, it belongs to II, but we wish to emphasize its emergence). This invariant curve can

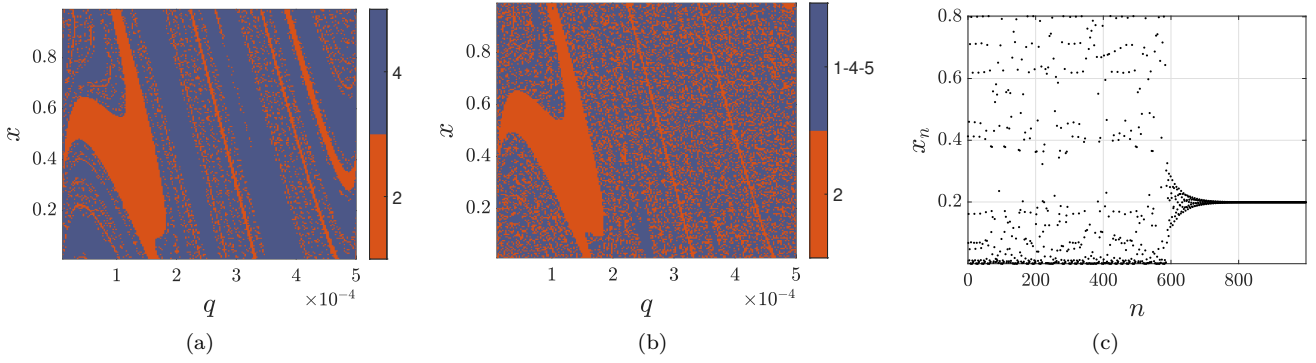


Figure 5: (a) Basins of attraction with $a = 17.54$ and $k = 0.865$: the chaotic attractor of family IV and the equilibrium coexist. (b) Basins of attraction with $a = 18.245$ and $k = 0.865$: a high-period orbit of the I-IV-V family and the equilibrium coexist. In both cases the numerical labels correspond to the Roman-numeral family indices, defined in Table 1. Note that the basins are intermingled. (c) Illustration of the transient chaos of an orbit converging to the equilibrium due to the I-IV-V chaotic saddle.

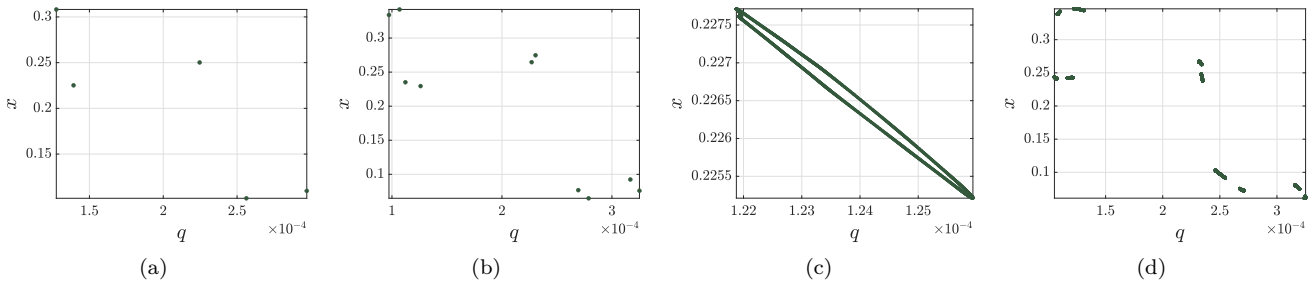


Figure 6: The various attractors of the II-5 family in the phase space. (a) The attractor is a period-five orbit. (b) The attractor is a period-ten orbit, born at the PD2-5 curve of Fig. 1. (c) The attractor is an invariant curve for the tenth iterate of the map, born at the NS2-5 curve of Fig. 1. (d) The attractor is chaotic after the period-doubling cascade.

be seen in Fig. 2(b), (c), Fig. 8, and Fig. 7; more detailed discussion on these figures will follow next. Saddle-node bifurcations originating from phase-locking on the primary NS_2^1 curve are crossed (cf. the saddle-node SN_{2-i} curves in Fig. 1), resulting in the appearance of cycles of various periods. We call the families of these orbits II- i in Table 1, with i representing their period, to stress that they are associated with the invariant curve, which in turn is connected to the equilibrium. In Fig. 1 the eight, five, seven and nine period tongues are illustrated. Near NS_2^1 , the Arnold tongues do not overlap; however, as the parameters move farther away from it, global bifurcation phenomena may lead to the coexistence of attractors originating from different tongues. These dynamical phenomena are qualitatively similar across all II- i type attractors. For this reason, we first describe the generic scenario and then provide representative examples of specific II- i orbits in what follows.

First note that the Arnold tongues are wider as the period of the resulting periodic orbit is lower. A 1 : 1 resonance with positive normal-form coefficient—denoted by R_1 in Fig. 1—, i.e. a co-dimension-2 point where both multipliers are equal to 1, is found on the upper branch of the tongue. Co-dimension-2 resonances act as organizing centers for the dynamics of the system. Crossing the saddle-node curves defining the upper branch from the left of R_1 , a stable cycle is born, which, as we move around R_1 , is destroyed in a NS bifurcation emanating from the R_1 point and a saddle invariant curve is born. We note that homoclinic structure are present near this point implying the birth and destruction of infinitely many long-period saddle cycles [45]. Inside the tongue, the corresponding periodic orbit—because it is possible for other orbits to coexist as the tongues overlap—undergoes a period-doubling route to chaos, and ultimately the family is destroyed through a boundary crisis. In Figs. 1 and 9, the first period-doubling curves in the Feigenbaum cascade of the five, seven, eight and nine Arnold tongues are shown. It is worth noting that a 1 : 2 resonance with negative normal form coefficient—denoted by R_2 in Fig. 1—, i.e. a co-dimension-2 point where both multipliers are equal to -1, is found on the upper branch of the PD curve. Similar to the R_1 resonance, this point acts as an organizing center for the dynamics of the system. The NS curve, crossing which results in the destruction of the stable cycle and the birth of a saddle invariant curve, connects the two co-dimension-2 points of the same family. Crossing the PD curve above the R_2 point results in the creation of an unstable period-doubled orbit, which gains stability as another NS curve emanating from the R_2 point is crossed. Within the region defined by the PD and (the second) NS curves, a stable invariant curve for the iterate of the map corresponding to the double period of the tongue is present. Similar to the 1 : 1 resonance, near the R_2 point infinitely many long-period

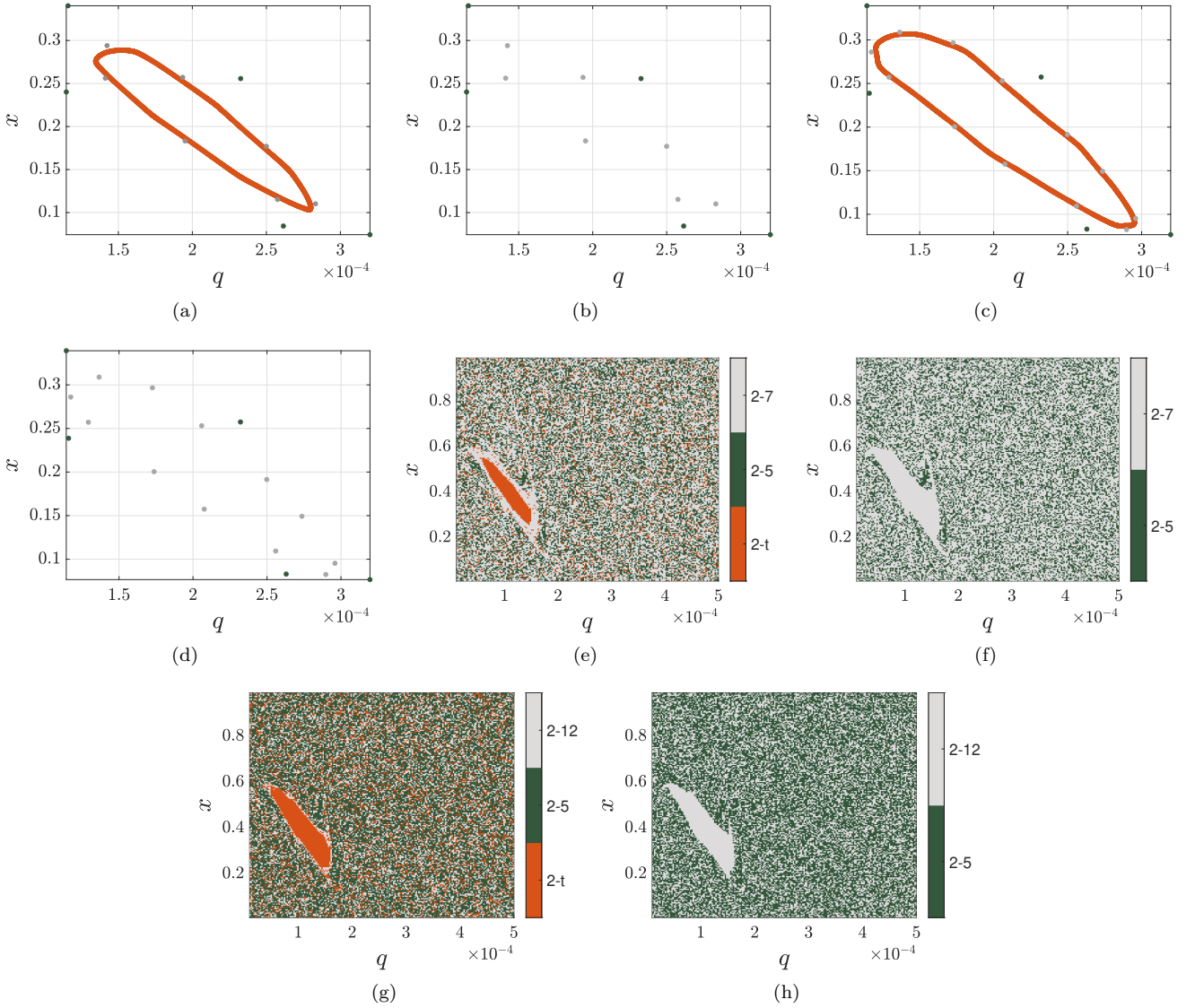


Figure 7: Phase space (a)-(d) and associated basins of attraction (e)-(h) with $a = 19.3$ fixed, corresponding to Fig. 2(c). The numerical labels 1, 2, ... correspond to the Roman-numeral family indices, defined in Table 1. (a) and (e): $k = 0.8706$, the period-five attractor of the II-5 family, the period-seven attractor of the II-7 family, and the stable invariant curve coexist. (b) and (f): $k = 0.8708$, the period-five attractor of the II-5 family and the period-seven attractor of the II-7 family coexist; the invariant curve has been destroyed. (c) and (g): $k = 0.8744$, the period-five attractor of the II-5 family, the period-twelve attractor of the II-12 family, and the reemerged invariant curve coexist. (d) and (h): $k = 0.8747$, the period-five attractor of the II-5 family and the period-twelve attractor of the II-12 family coexist; the invariant curve has again been destroyed. In all cases, note again the intermingling of the basins.

unstable cycles appear and disappear due to the involved homoclinic structures [45]. The region around the NS curve of the fixed point is filled with overlapping resonance structures of the above-described type, thus implying multistability among the corresponding periodic cycles.

To illustrate the bifurcations involving each of the II- i cycles described above, we consider, indicatively, the five-period cycle, illustrated in Fig. 6(a), created upon crossing SN_{2-5} , which is also the first resonance attractor in Fig. 2. Referring to Fig. 1, this cycle exists in the region defined by the two branches of the five-Arnold tongue, the curves PD_{2-5} and NS_{2-5} connecting the two codimension-2 resonance points. When the parameters cross SN_{2-5} comprising the tongue, the cycle collides with a saddle orbit and disappears, while when the parameters cross NS_{2-5} , a saddle invariant curve for the fifth iterate of the map is created. The crossing of PD_{2-5} results in a cycle of ten period shown in Fig. 6(b). The transverse homoclinic tangle implies the existence of horseshoe-like dynamics near the R_1 point, but the chaotic invariant set is non-attracting due to the sign of the normal-form coefficient. From the R_2 resonance point lying on PD_{2-5} , apart from NS_{2-5} connecting it with the R_1 point, another NS curve emanates (not shown in Fig. 1), which upon crossing results in the birth of stable invariant curve for the tenth iterate of the map, illustrated in Fig. 6(c). The Feigenbaum cascade of the period-five cycle leads to the formation

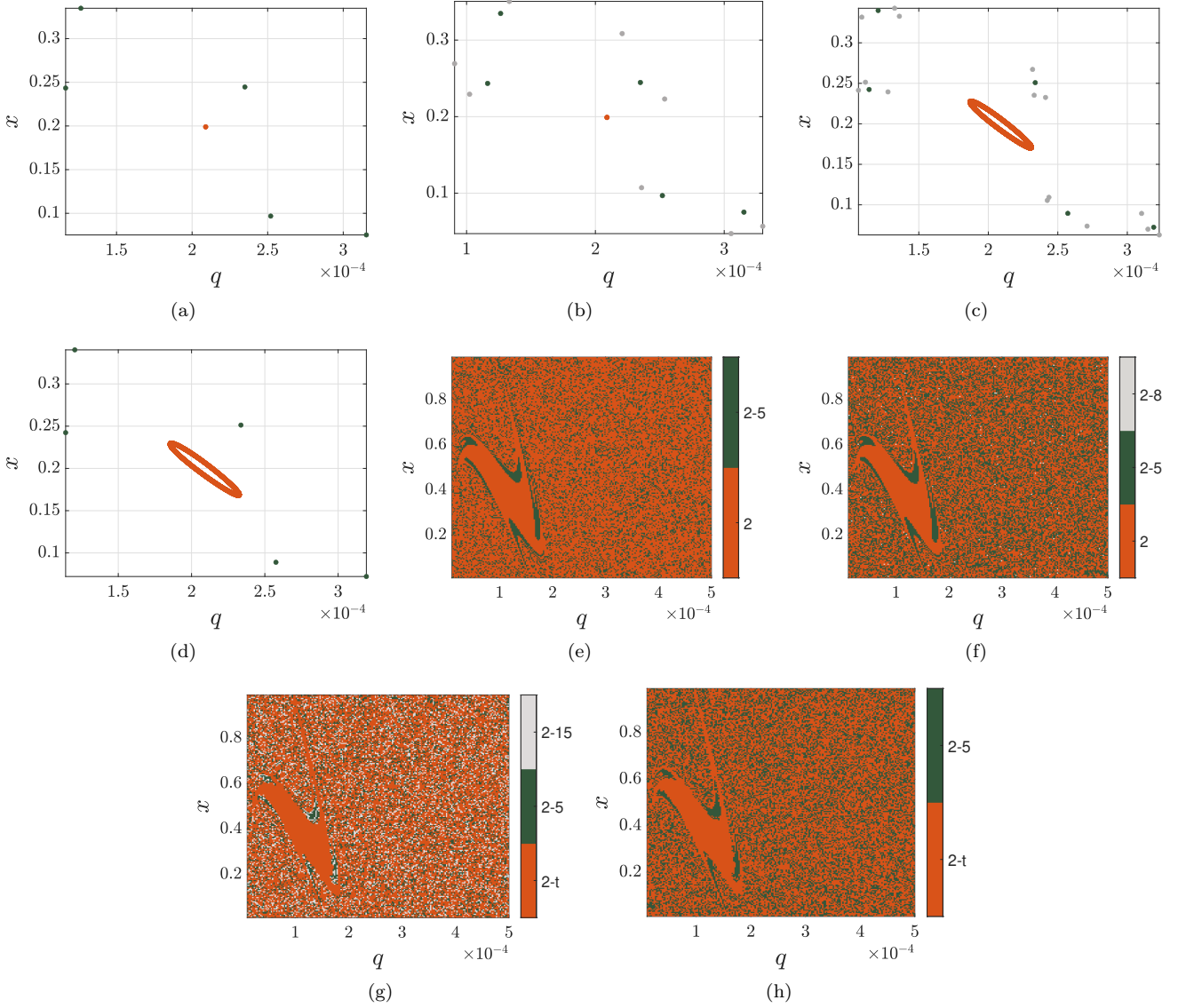


Figure 8: Phase space (a)-(d) and associated basins of attraction (e)-(h) with $k = 0.865$ fixed, corresponding to Fig. 2(b). The numerical labels 1, 2, ... correspond to the Roman-numeral family indices, defined in Table 1. (a) and (e): $a = 19$, the period-five attractor of the II-5 family and the equilibrium coexist. (b) and (f): $a = 19.0725$, the period-five attractor of the II-5 family, the period-eight attractor of the II-8 family, and the equilibrium coexist. (c) and (g): $a = 19.221$ the period-five attractor of the II-5 family, the period-fifteen attractor of the II-15 family, and the equilibrium coexist. (d) and (h): $a = 19.2282$, the period-five attractor of the II-5 family and the equilibrium coexist. In all cases, note the intermingling of the basins.

of the chaotic attractor, shown in Fig. 6(d). We close noting that the dynamical phenomena described above are shared by all the attractors of II- i type, as also indicated by inspecting the bifurcation curves in Fig. 1.

The Neimark-Sacker curve NS_2^1 of the fixed point has itself a codimension-2 R_2 resonance point, which, as previously discussed, also acts as an organizing center. Beyond this point, NS_2^1 essentially no longer corresponds to a Neimark-Sacker bifurcation, but rather to a neutral saddle. As shown in Fig. 1, a PD curve—denoted by PD_2 —crosses NS_2^1 at the R_2 point; crossing it from below R_2 results in the emergence of a stable period-two orbit. However, crossing it from above results in the creation of a saddle period-two orbit, which gains stability after crossing another NS curve (NS_2^2) emanating from the R_2 point and connecting it with an R_1 point on the PD curve of the period-two cycle (c.f. Fig. 9). At this curve, a period-doubled cycle that was born upon crossing PD_2 below R_2 is correspondingly destroyed. The NS_2^2 curve in question will also be discussed in the next subsection, in the examination of the second region of the parameter space, since for the parameter value $k = 0.865$ considered here the stable period-two orbit is created in the second parameter region.

Returning to Fig. 2 (b), the emerging attractors can be grouped into the following types: II (equilibrium), I-IV-V and II- i . The first resonance attractor is the five-period cycle discussed above. The phase space, in the case where only this cycle and the equilibrium coexist as attractors, is shown in Fig. 8(a) and the associated basins

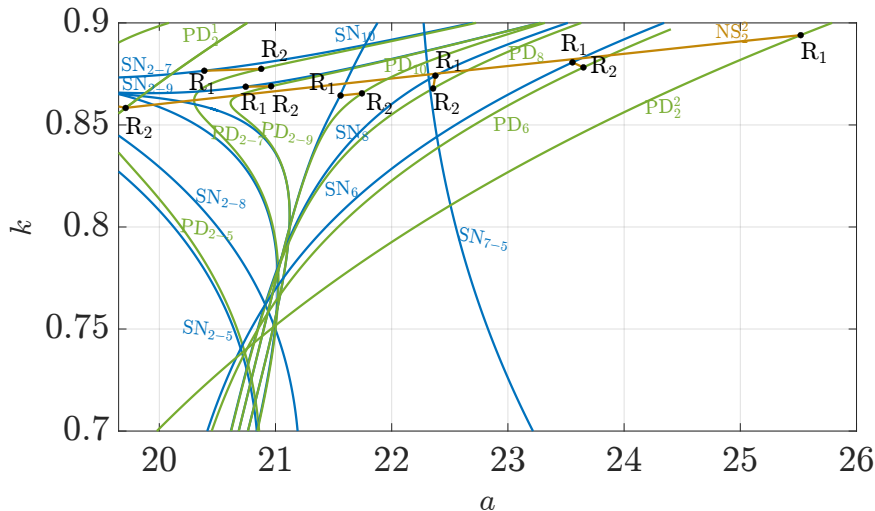


Figure 9: Bifurcation curves in the second region. Saddle-node bifurcations are denoted by SN, period-doubling bifurcations by PD, and Neimark-Sacker bifurcations by NS. Bifurcation curves of the same type share the same color. The index of each curve refers to the attractor family of Table 1. For clarity, the SN_{6-j} curves are denoted by SN_j , while the labels of the NS curves connecting R_1 and R_2 points are, except NS_2^2 , have been omitted. The superscript in the PD and NS curves refers to their order in the respective family. The labels R_1 correspond to 1 : 1 strong resonances, while the labels R_2 to 1 : 2 strong resonances.

of attraction in Fig. 8 (e). As is visually apparent, the entropies in Table 2 have increased, confirming the more complex nature of the basins of attraction. Its corresponding tongue overlaps with, and in fact contains, several of the remaining tongues, suggesting that multistability, along with other resonance periodic orbits, will be observed. Several examples are shown in Fig. 2(b): as a varies, the parameters first enter the region of the eight-Arnold tongue, shown in Fig. 1, giving rise to a period-eight cycle which, following the generic pattern discussed previously, ultimately leads to the formation of a chaotic saddle. The phase space in which the II-8 family period-eight cycle coexists with the II-5 family period-five cycle and the fixed point is shown in Fig. 8(b). It is worth noting that the basin of attraction of the eight-cycle, as shown in Fig. 8(f) is essentially intermingled within the basins of the other attractors. Similar considerations apply to the other resonance higher-order periodic orbits shown in Fig. 2. When the parameters ultimately cross NS_2^2 , the equilibrium loses stability and a stable invariant curve emerges, coexisting with the II- i attractors. Note that because the parameter values are far from the points from which the Arnold tongues emanate, the corresponding periodic orbits are no longer necessarily close to the invariant curve in a geometric sense, as shown for example in Fig. 8 (g) and (h). The basins of attraction of the invariant curve coexisting with the II-5 and II-15 attractors, and with the II-5 attractor after the destruction of the II-15 one, are shown in Fig. 5(e) and (f). It is worth noting that the basin and boundary basin entropies attain high values in the first case and decrease in the latter case, while still remaining above the fractality threshold—cf. Table 2.

Concluding the study of the parameter region of Fig. 1, we note that for large values of k no periodic attractors exist, as all have been destroyed by the upper branch of the corresponding Arnold tongue. However, the chaotic saddle, which as marked in Fig. 10(c) causes transient chaos, becomes attracting when the basin boundary is crossed in parameter space, namely through a reverse boundary crisis. The chaotic attractor remains the sole attractor of the system for large k . Fig. 2(c) shows the bifurcations involving the various periodic attractors, the invariant curve, as well as the emergence of the chaotic attractor, as $a = 19.3$ is fixed and k increases. We note that the invariant curve undergoes a sequence of global bifurcations associated with its collision with the stable manifold of a resonant saddle cycle, its reappearance through the reverse process, and its final destruction. Fig. 7 shows the phase space and the basins of attraction of the coexisting attractors as the bifurcations of the invariant curve unfold. It is worth noting that the II-7 and II-12 periodic attractors appear very close to the invariant curve as a result of their proximity to the corresponding Arnold tongues; cf., in contrast, the II-5 cycle. Moreover, the entropies in Table 2 attain high values, especially in the case of three coexisting attractors shown in Fig. 7(c), confirming the visual complexity of the basins of attraction shown in Fig. 7. The same situation will also arise in the following discussion, when the second region of the bifurcation diagram is examined.

3.2 Dynamics within the second region

We continue with the study of the second region of the parameter space, shown in Fig. 9. To illustrate the emerging attractors as the various bifurcations unfold, we fix $k = 0.865$ and vary the learning rate, i.e., a , focusing first on Fig. 10(a). As in the last region of Fig. 2(b), the invariant curve and the five-period orbit coexist for smaller values

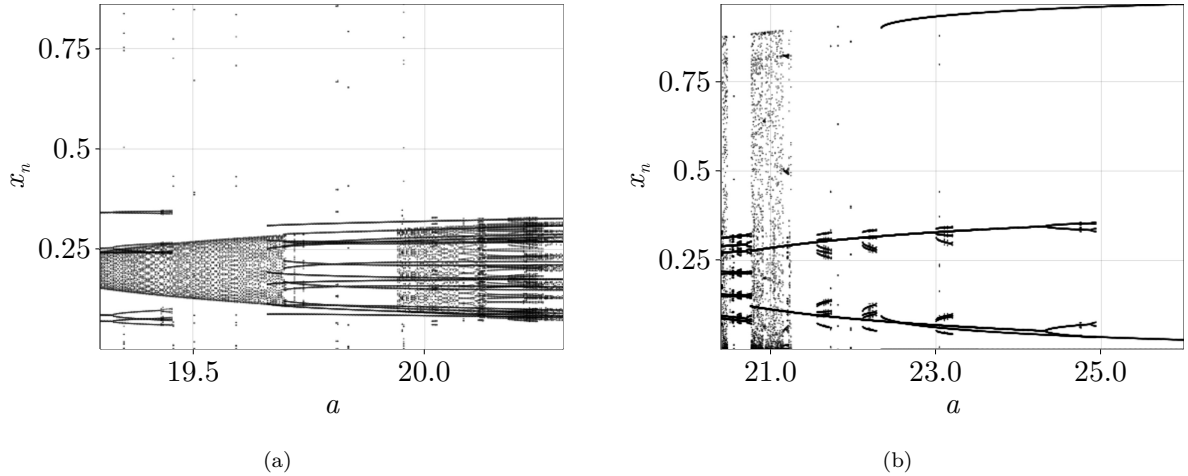


Figure 10: The various emerging attractors as $k = 0.865$ is held fixed and a is gradually increased. Each attractor's birth or destruction corresponds to the crossing of a bifurcation curve of Fig. 9 or to a crisis.

of a , with the latter undergoing a period-doubling route to chaos as each of the PD curves is crossed, the first of which is shown in Fig. 9. Of course, within very narrow regions of the parameter space, we observe periodic attractors of the I-IV-V type, originating from the presence of the chaotic saddle. As the parameters enter the seven- and nine-Arnold tongues, shown in Fig. 9, the corresponding periodic cycles appear. Note at this point that the tongues have the qualitative structure discussed previously: the upper branch exhibits a codimension-2 R_1 resonance from which an NS curve emanates (not labeled in Fig. 9 for the sake of clarity), connecting it with a codimension-2 R_2 resonance point located on the PD curve of the corresponding cycle of the tongue. The dynamics induced by this structure is qualitatively similar to that discussed for the five-period cycle.

The invariant curve, born at NS_2^1 follows the familiar bifurcation pattern of disappearing and reappearing already encountered in the examination of the first region. For higher values of a , we observe the coexistence of several different periodic orbits with overlapping resonant tongues (not shown for clarity in Fig. 9). An indicative example of overlap between the seven- and nine-tongues (shown in Fig. 9) and those of periods 16 and 25 is presented in Fig. 11, which illustrates in (a) the phase space and in (b) the complexity of the basins of attraction. Apart from the obvious high values of the entropies, it is worth noting that in this case $S_b = S_{bb}$, meaning that every point in the basin is actually a boundary point. This represents an interesting case of complete mixing with $S_b = S_{bb}$, but characterized by non-intermingled boundaries [24], as the entropies are not equal to the Wada index [24]—which is also visually apparent from the figure.

The presence of both the I-IV-V and II- i chaotic saddles results in large transiently chaotic intervals; Fig. 11(c) shows an orbit spending a long time near the regions of the I-IV-V and II-25 chaotic saddles before finally converging to the seven-cycle. As expected, the seven-cycle undergoes a period-doubling route to chaos (the first PD curve, PD_{2-7} is shown in Fig. 9), following the generic pattern of the II- i family of attractors. The time spent near the saddles gradually increases, and eventually the I-IV-V chaotic saddle gains stability via a reverse boundary crisis bifurcation—cf. Fig. 10(b). The phase space and the basins of attraction when the chaotic attractor coexists with the nine-period cycle are shown in Fig. 12(a) and (d), respectively—note that the basin of the nine-cycle can be loosely thought of as being organized around the (unstable) invariant curve and that S_b attains a significantly low value, while $S_{bb} < 0.439$. Moreover, geometrically the nine-cycle captures roughly the region of the invariant curve. As illustrated in Fig. 10(b), further increasing a results in the destruction of the I-IV-V attractor through a boundary crisis, as well as in the emergence and disappearance of other high-period orbits as the corresponding tongues are crossed. After the destruction of the II-9 attractor, the chaotic attractor reemerges and coexists with a period-two cycle.

Regarding this two cycle, we note that as also discussed previously, NS_2^1 exhibits a codimension-2 R_2 resonance point through which PD_2^1 passes. Since, for the value of k under consideration, the PD curve is crossed from above, the initially emerging period-two orbit is of saddle type. It gains stability, corresponding to the attractor of Fig. 10(b), upon crossing NS_2^2 emanating from the R_2 point and connecting it with an R_1 resonance point on the PD curve of the corresponding period-two orbit, denoted by PD_2^2 . Since it originates from the the fixed point and to highlight its difference from the II- i families, we continue to denote its by family II. Its basin of attraction, shown in Fig. 12(e), is organized around the around the two points of the cycle (cf. the phase space in Fig. 12 (b)) and, as is expected, the associated entropies attain significantly lower values compared to the cases of intermingled basins discussed earlier. We note that although the structure organized around the R_2 point appears similar to that examined in the case of the Arnold tongues, the normal-form coefficient in this case is positive; thus, the

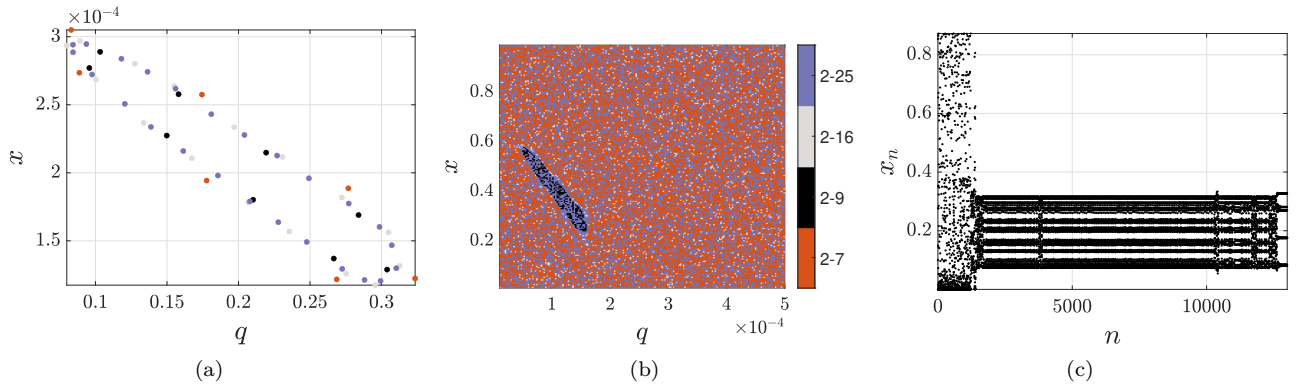


Figure 11: Coexisting II–7, I–9, II–16, and I–25 attractors in the phase space (a) and their basins of attraction in (b), $a = 20.14$, $k = 0.865$. Note the intermingling of the basins. (c) Transient chaos due to the I–IV–V and II– i chaotic saddles of an orbit converging to the period-seven attractor.

two-invariant curve that is destroyed when the period-two orbit gains stability is not stable.

As the parameters vary further (cf. Fig. 10), the chaotic attractor transitions to periodic behavior through a boundary crisis, with the periodic orbit undergoing a Feigenbaum route to chaos. The original chaotic attractor reemerges through a reverse boundary crisis and is ultimately destroyed through another boundary crisis, leaving the period-2 orbit as the sole attractor. Increasing a , a stable ten-cycle is born at the SN_{10} curve of Fig. 9, as shown in Fig. 10(b) and in Fig. 12(c). Its basin of attraction is intermingled with that of the period-two cycle—cf. Fig. 12(g) and Table 2, yet S_b is small. The origin of this periodic attractor, however, is not the phase-locking Arnold tongues of the invariant curve encountered so far; for this reason, we denote its family by VI in Table 1. For clarity, we use as index in the associated bifurcations of the family in Fig. 9 the period of the cycle instead of $6 - 10$. The SN curve exhibits a codimension-2 R_1 point, following a similar generic structure to that of the primary PD_2^1 curve. As the parameters cross PD_{10} , the orbit undergoes period-doubling, while the resulting twenty-cycle is destroyed in a boundary bifurcation before the VI family transitions to chaos. Attractors of the I–IV–V family also exist within narrow parameter regions, as is clear from Fig. 10(b).

The eight- and six-period cycles appearing as their corresponding SN_8 and SN_6 curves in Fig. 9 are crossed, as well as other high-period cycles existing within very narrow parameter regions and shown in Fig. 10(b), follow qualitatively similar behavior to that of the ten-period cycle discussed above. For this reason, with slight abuse of notation, we also denote the families of these attractors again by VI and use as index their corresponding period. However, the period-five cycle born at SN_{7-5} (c.f. Fig. 9) and shown in Fig. 10(b), VII family of Table 1, does not undergo any further bifurcation; accordingly, its SN curve exhibits no codimension-2 resonances. In fact, it remains the sole attractor of the system for sufficiently large learning rate a , after the period-2 orbit period-doubles twice and is ultimately destroyed in a boundary crisis (before transitioning to chaos, similarly to the VI families). The phase space and the basins of attraction when the period-two II and period-five VII attractors coexist are shown in Fig. 12(d) and Fig. 12(h). It is worth noting that apart from a decrease in the S_{bb} , suggesting that the basin boundary possesses no more a fractal nature, the five-period cycle captures most of the phase space, which, prior to its emergence, belonged to the basin of the two-period cycle. After the destruction of the family II attractor, this period-five cycle remains the sole attractor of the system for large a .

Summarizing the dynamics analyzed in the two regions shown in Figs. 1 and 9, we emphasize that, despite the complexity of the bifurcations occurring in the system, the attractors can be grouped and systematically classified into seven families, as reported in Table 1. A high-level overview of the key aspects of the dynamics is as follows: the I, III, IV and V families originate from period-three, period-nine, period-four, and period-seven respectively cycles, which undergo period-doubling cascades to chaos, transition to chaotic saddles after boundary crises, and eventually merge, forming a merged chaotic saddle. Within narrow parameter regions, periodic orbits located near the chaotic saddle gain stability and are subsequently destroyed in boundary crises. Transiently chaotic behavior also observed and traces back to the chaotic saddle.

The fixed point (family II) is stable, coexisting with the attractors of the I, III, IV, or the merged I/III/IV family—and we emphasize this in contrast to the traditional MWU algorithm, in which, when the fixed point is stable, it is also the unique global attractor of the system—until it loses stability via an NS or a PD bifurcation, c.f. the curves NS_2^1 and PD_2 . The two curves meet at an R_2 codimension-2 resonance point. The NS curve, which results in a stable invariant curve when crossed above the R_2 point, induces overlapping phase-locking Arnold tongues, leading to the birth and coexistence of periodic orbits belonging to the II– i family. Each of these tongues is characterized by qualitatively similar behavior in terms of codimension-2 resonances (R_1 on the upper branch of the tongue and R_2 on the first PD curve) and in terms of the underlying bifurcations of each II– i attractor, involving Feigenbaum

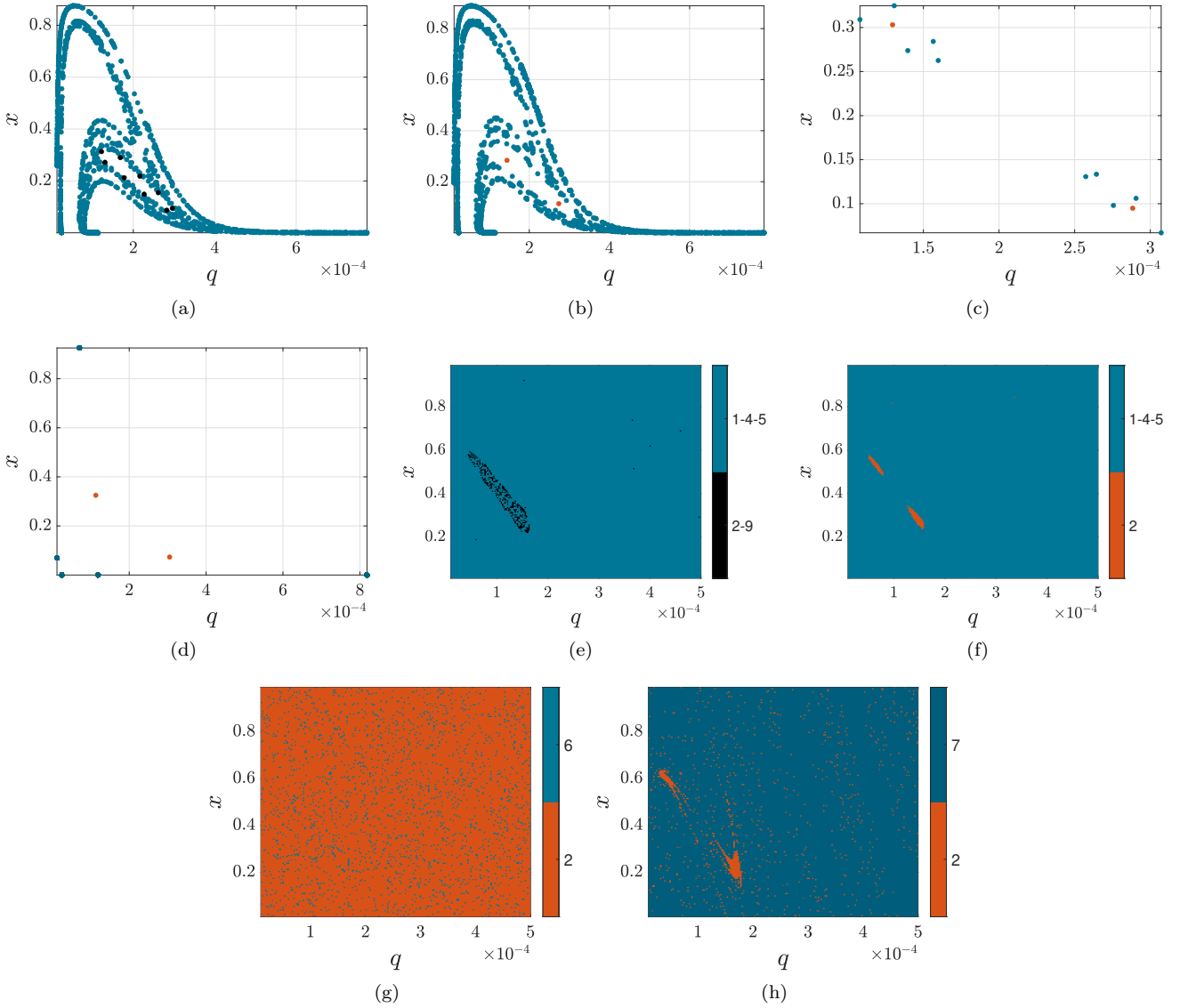


Figure 12: Phase space (a)-(d) and associated basins of attraction (e)-(h) with $k = 0.865$ fixed, corresponding to Fig. 10 (a) and (b). The numerical labels 1, 2, ... correspond to the Roman-numeral family indices, defined in Table 1. (a) and (e): $a = 20.43$, the period-nine attractor of the II-9 family and the chaotic attractor of the I-IV-V family coexist. (b) and (f): $a = 20.97$, the period-two attractor of the II family and the chaotic attractor of the I-IV-V family coexist. (c) and (g): $a = 21.64$, the period-two attractor of the II family and period-ten attractor of the VI family coexist. (d) and (h): $a = 22.75$, the period-two attractor of the II family and period-five attractor of the VII family coexist.

routes to chaos and destruction via boundary crises. The basin boundaries of the coexisting attractors are always fractal and highly intermingled.

As the several II- i attractors appear and disappear and the invariant curve is destroyed, the I/III/IV chaotic saddle regains stability within certain parameter regions. The codimension-two points of the period-two orbit, although structurally similar to those of the tongues, are characterized by an opposite normal-form coefficient at the R_2 point; thus, when the primary NS curve, i.e. NS_2^1 , is crossed above the R_2 point, the period-two cycle is born as a saddle at PD_2 and gains stability when the secondary NS curve is crossed. The periodic orbits of the VI family, which do not originate from phase-locking tongues and appear as their SN curves are crossed, exhibit a similar pattern concerning the codimension-two points as described above. They are destroyed in a boundary crisis before transitioning to chaos. Similarly, the period-two cycle undergoes two period-doublings and is destroyed in a boundary crisis.

The system is thus left with a single, global, period-five attractor of the VII family, initially coexisting with the II and VI attractor families. This attractor undergoes no further bifurcations, and beyond the destruction of the period-two cycle, no attractors belonging either to the existing families or to new families are born. In fact, the behavior of the system for sufficiently large learning rate is predictable, and we highlight this property as being in stark contrast to the standard MWU, in the absence of extreme events.

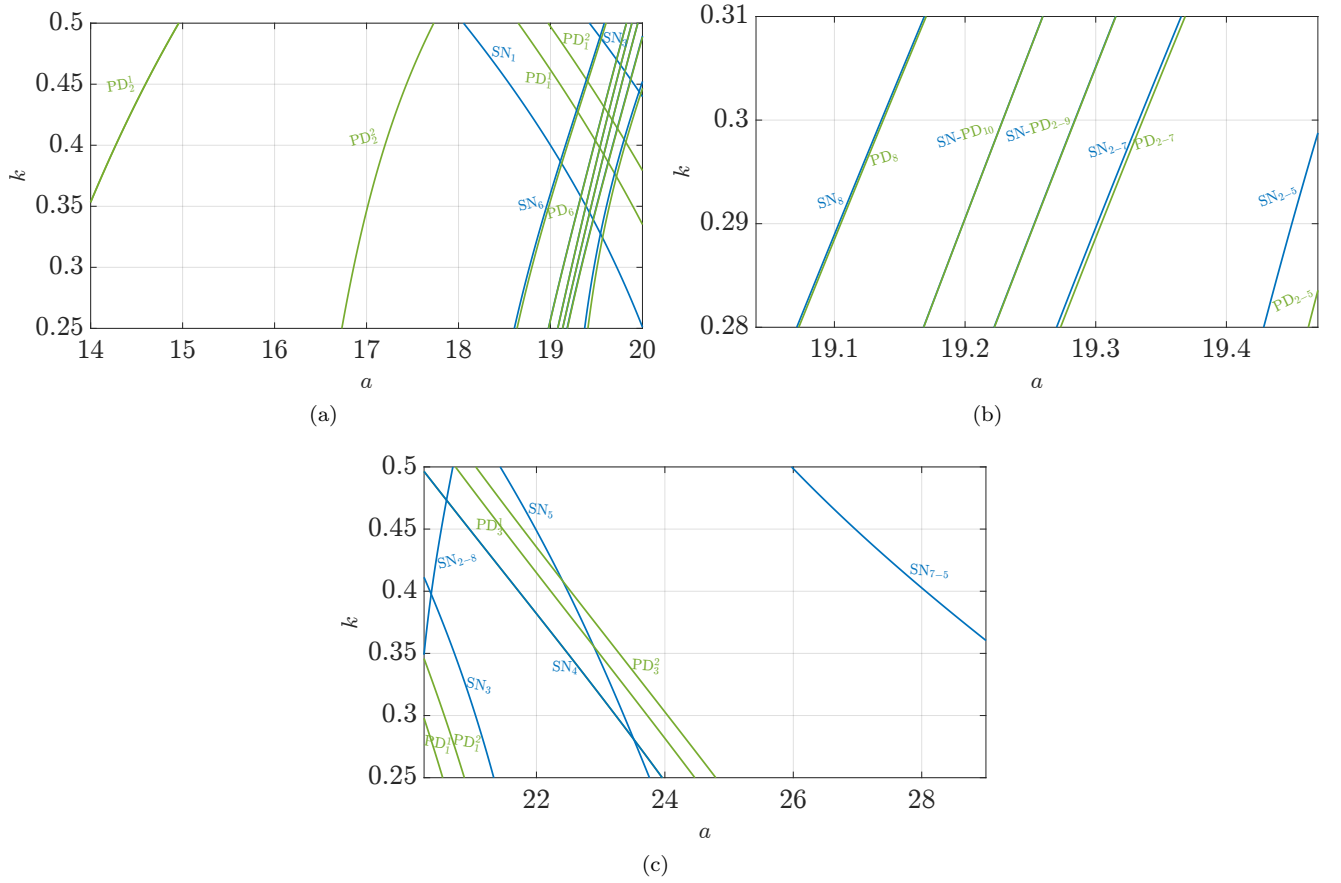


Figure 13: Bifurcation curves in the third region, divided into two subregions shown in (a) and (c). In (b), an enlarged version of (a) is shown for clarity. Saddle-node bifurcations are denoted by SN and period-doubling bifurcations by PD. The index of each curve refers to the attractor family of Table 1. Bifurcation curves of the same type share the same color. For clarity, the SN_{6-j} curves are denoted by SN_j . The superscript in the PD curves refers to their order in the cascade. Some SN and PD curves in (b) are so close that they are indistinguishable.

3.3 Dynamics within the third region

From the discussion of the two regions above, we have essentially exhausted all possible bifurcations of the system, and all primary attractor families have been identified. The purpose of this subsection is not to illustrate new bifurcations, but to show how the order of emergence, the type, and the coexistence of attractors change depending on how each bifurcation curve is crossed. Moreover, it is shown that the different order of bifurcations leads to different merged attractor families, in a similar manner to the I/III/IV discussed previously. To this end, in what follows we fix $k = 0.3$. The bifurcation curves are shown in Fig. 13, while Fig. 14 shows the emerging attractors as the parameter a varies.

Because of the choice of the value of k and based on the above discussion and Figs. 1 and 9, we know that the fixed point will not undergo an NS bifurcation; instead, a period-two cycle will emerge upon crossing PD_2 . As is evident from Figs. 13 and 14(a), the cascade of period-doublings of the fixed point, namely of the II family, unfolds before any attractor belonging to a different family appears. In fact, a two-piece chaotic attractor emerges, which after an interior crisis expands into a one-piece attractor. This should be contrasted with the situation discussed in the previous subsections, where the period-doubled orbits were destroyed before transitioning to chaos, while coexistence with other families was also observed.

As a increases, the SN curve of the period-six orbit of the VI family is crossed. This results in the appearance of a stable period-six orbit, while the chaotic attractor is destroyed through a boundary crisis—cf. the enlarged version in Fig. 14(b).

This orbit then undergoes a period-doubling route to chaos, after which the chaotic attractor reemerges. As a result, the period-six cycle belongs to the same branch as the chaotic attractor, appearing as a periodic window. This property is in fact true for all the II- i and VI periodic attractor families studied in the previous subsections. Thus, none of these families coexist with each other or with the chaotic attractor; rather, they are all embedded as periodic windows in the chaotic branch of the II family and undergo period-doubling route to chaos before the chaotic attractor reemerges. The enlarged version of Fig. 14(c) shows two examples of periodic windows of the

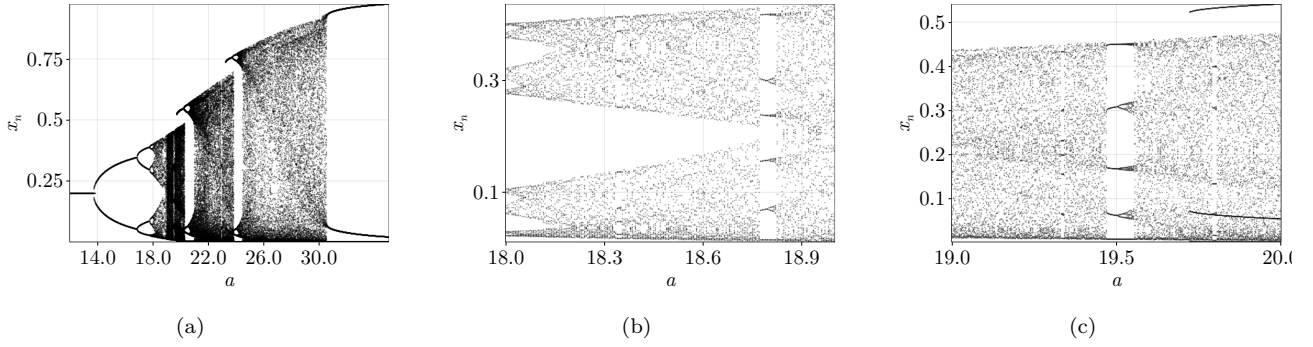


Figure 14: (a) The various emerging attractors as $k = 0.3$ is held fixed and a is gradually increased. Each attractor's birth or destruction corresponds to the crossing of a bifurcation curve of Fig. 13 or to a crisis. (b) and (c) correspond to enlarged versions of (a), highlighting the boundary and interior crises as well as the transition between periodic and chaotic behavior.

II-5 and II-7 families. Note that the proximity of the NS and PD bifurcation curves in Fig. 14(b) implies that the corresponding periodic windows are very narrow and are difficult to distinguish. We also note that the order of appearance of each of these attractors now differs, as it depends on the order in which the corresponding SN curves of Fig. 13 are crossed.

However, the I, III, IV, and V families do not follow the above-discussed pattern, as they coexist with the chaotic attractor after their appearance. As shown in Fig. 10(c) and Fig. 14(a), the period-three attractor of family I, born at NS_3 Fig. 13, coexists with the chaotic attractor, which becomes a chaotic saddle after a boundary crisis. The period-three orbit undergoes period-doubling to chaos and merges with the II family chaotic saddle, forming a larger chaotic attractor of the merged family I/II.

This attractor follows a similar pattern, exhibiting narrow periodic windows, coexisting with the four-period IV cycle, and ultimately transforming into a chaotic saddle through a boundary crisis. Correspondingly, the period-four attractor undergoes period-doubling route to chaos and expands, incorporating the chaotic saddle I/II via an interior crisis, thus forming a larger chaotic attractor of the merged family I/II/IV. We note that the III and V families appear alone only within very narrow windows before merging into the larger attractor; for this reason, we omit them from the notation of the merged attractor. The merged attractor is now qualitatively similar to that of family I/II/IV discussed in the previous sections. The chaotic regime ends with the birth of the V family period-five attractor, which becomes the sole attractor of the system for large a , as expected from the analysis of the previous sections.

3.4 A note on different choices of fixed parameters

In this subsection, we briefly elaborate on the initial statement of the present Section regarding the changes in the system dynamics when different fixed parameters are chosen. The fixed point always undergoes a PD bifurcation similar to the PD_2^1 curve discussed previously. On this curve lies a codimension-two R_2 point, which may not lie within the admissible parameter set, i.e., $k \in [0, 1]$. As a result, the NS curve crossing this point may lie outside the admissible parameter region. In that case, no stable invariant curve is created, and the bifurcation diagram has a structure similar to Fig. 13. The overall dynamics can then be analyzed as in Subsection 3.3, and Fig. 14 can be regarded as a generic picture. Otherwise, if the NS curve does lie within the admissible parameter region, the generic picture of Figs. 1, 9, and 13, as well as the analysis conducted in the corresponding sections, applies. Note, however, that the exact periods of the periodic orbits may differ. Thus, when the extreme event is characterized by different parameters, the analysis can be carried out in a similar manner, and no qualitatively new phenomena are expected; only quantitative differences in the bifurcation curves arise.

As an example, we consider the fixed parameters $b = 0.3$, $p_0 = p_1 = 10^{-5}$, $\alpha = 0.97$, $M = 35$. For these parameter choices, the NS_2^1 curve of the fixed point does not lie within the admissible parameter region. As a result, we expect behavior similar to that discussed in Section 3.3. Inspecting Fig. 15, we indeed observe qualitative similarity with Fig. 14(a). Apart from the quantitative differences regarding the critical parameter values at which each attractor appears, note that the periodic attractor born after the boundary crisis of the chaotic attractor, although it does not undergo any further bifurcations similarly to the period-five VII attractor discussed in the previous sections, has period seven.

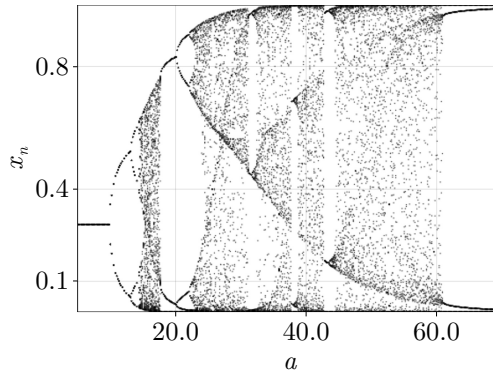


Figure 15: Attractors as a varies and $k = 0.865$ for the different set of fixed parameters.

4 Summary and conclusions

In this paper, we studied the nonlinear dynamics of a risk-sensitive variant of the Multiplicative Weights Update (MWU) for two-strategy population congestion games in the presence of extreme events affecting the first resource. Agents are assumed to learn and react to the perceived risk, captured by a belief variable. This variable is updated through a standard discrete-time adaptive expectation rule that accounts for the risk signal generated by the environment. The population state evolves according to the MWU, incorporating the agent’s belief about the risk of the first resource. As a result, the learning dynamics becomes two-dimensional.

Dynamically, the system always admits two trivial boundary equilibria, one of which is always a saddle, while the stability of the other depends on the parameters; when stable, it is the global attractor. The nontrivial regime arises when both boundary equilibria are saddle and an interior equilibrium exists, which is stationary from a game-theoretic perspective. In that case, a detailed two-parameter bifurcation analysis with respect to the parameters controlled by the agents is conducted to identify regions of qualitatively different behavior. Despite the complexity of the dynamics, the attractors of the system can be grouped into specific families.

The fixed point loses stability via either a supercritical period-doubling (PD) or Neimark-Sacker (NS) bifurcation—the latter being absent in one-dimensional variants of MWU. Unlike the traditional MWU dynamics, in its stable regime the fixed point coexists with different families of attractors. These families originate from periodic orbits, undergo Feigenbaum cascades to chaos, crisis bifurcations and merging, giving rise to transient chaos and narrow periodic windows. The stable invariant curve born at the NS bifurcation of the fixed point leads to the creation of infinitely many Arnold tongues. The phase locking also constitutes a new phenomenon that has not been identified in traditional MWU dynamics, even in the heterogeneous setting.

The dynamics within each tongue is qualitatively similar: PD and NS bifurcations occur, while codimension-two points serve as organizing centers. Similar codimension-two structures are observed for the period-two cycle originating from the fixed point. The overlap of different tongues results in coexistence among multiple periodic attractors as well as the invariant curve, with intermingled basins of attraction. As the learning rate increases, each family is destroyed through boundary crises, except for a period-five cycle which remains the sole attractor of the system. Variations of the fixed parameters result in qualitatively similar dynamics, making the described picture generic. Despite the complexity of the dynamics, the time-averages of the trajectories are proved to converge to the stationary equilibrium, similarly to the traditional MWU algorithm.

We highlight that incorporating the risk associated with the extreme event into the decision-making process leads to the emergence of several phenomena that are absent from the MWU variants studied so far. These include invariant curves appearing as attractors, phase-locking phenomena, and codimension-two resonances. Notably, the stationary interior equilibrium may be stable while coexisting with both chaotic and periodic attractors. Moreover, for large values of the learning rate, the system exhibits predictable periodic behavior, in contrast to traditional MWU variants.

This work aims to serve as a first step toward understanding the effect of extreme events, and more generally the coupling of game dynamics with a belief variable. Several directions remain to be explored. We highlight two major avenues. The first concerns the risk-sensitive analysis of other classes of games; for instance, one could study the effect of extreme events as perturbations of zero-sum games under replicator dynamics, where the unperturbed system possesses a Hamiltonian structure. The second involves stochastic models in which extreme events directly perturb the game dynamics, rather than being incorporated through a deterministic risk-sensitive correction, with particular emphasis on the resulting large-deviation estimates.

Acknowledgement

This work has been supported through a Vannevar Bush Faculty Fellowship administered through the ONR Award N000142512059.

Competing interests

The authors have no relevant financial or non-financial interests to disclose.

Data availability

No datasets were generated or analysed during the current study.

A Omitted details from Section 2.3

In this appendix, we provide the technical details omitted from Section 2.3 regarding the boundary equilibria $(0, p_0)$ and $(1, p_0 + p_1)$, as well as the connection between the evaluation of the risk in (6) and the CVaR risk measure. In what follows it is always assumed that $x_0 \in (0, 1)$.

A.1 Boundary Equilibria

First, we show the following property regarding the boundary equilibria of (9), which was used in the proof of Proposition 1 and is also used in the proof of the global stability of $(0, p_0)$ in Lemma 2.

Lemma 1. *Let $x_0 \in (0, 1)$ and $q_0 \in (0, 1)$, then there exists a $\delta_1 \in (0, 1)$ such that $x_n < 1 - \delta_1$ for all $n \geq 0$. Furthermore, if $b > cp_0$, then there is a $\delta \in (0, 1)$ such that $x_n \in (\delta, 1 - \delta)$ for all n .*

Proof. For this proof it is more convenient to work with the logits $y_n = \log(x_n/(1 - x_n))$. Then, using (9) we have

$$y_{n+1} = y_n - a(x_n - b + cq_n).$$

Let $\varepsilon_1 = (1 - b)/2$. If $x_n \geq 1 - \varepsilon_1$, then $x_n - b + cq_n > 0$ and, thus, $y_{n+1} < y_n$, implying $x_{n+1} < x_n$. By continuity of the x -component of the map on the compact set $[0, 1 - \varepsilon_1] \times [0, 1]$, there exists $\mu < 1$ such that $x_n \leq \mu < 1$ whenever $(x_{n-1}, q_{n-1}) \in [0, 1 - \varepsilon_1] \times [0, 1]$. As a result, there is a $1 > \delta_1 > 0$ such that $x_n < 1 - \delta_1$ for all n .

Now suppose that $b > cp_0$. Let $\bar{q} \in (p_0, b/c)$ and $\varepsilon_2 > 0$ small enough so that

$$p_0 + p_1\varepsilon_2 < \bar{q}, \quad \varepsilon_2 - b + c\bar{q} < 0.$$

Let $\theta = p_0 + p_1\varepsilon_2 < \bar{q}$ and $\beta = b - c\bar{q} - \varepsilon_2 > 0$. If $x_n \leq \varepsilon_2$ and $q_n \leq \bar{q}$, then

$$x_n - b + cq_n \leq \varepsilon_2 - b + c\bar{q} = -\beta,$$

and hence $y_{n+1} \geq y_n + a\beta$. Thus, once x_n is sufficiently small and $q_n \leq \bar{q}$, the x -coordinate is pushed away from zero. It remains to control the indices for which $x_n \leq \varepsilon_2$ but q_n may still be larger than \bar{q} . Consider N indices such that $x_s, x_{s+1}, \dots, x_{s+N-1} \leq \varepsilon_2$. Then

$$q_{s+N} \leq (1 - k)^N q_s + (1 - (1 - k)^N)\theta \leq (1 - k)^N + (1 - (1 - k)^N)\theta.$$

But since $\theta < \bar{q}$, there is an $L \geq 1$ such that

$$(1 - k)^L + (1 - (1 - k)^L)\theta \leq \bar{q}.$$

As a result, if $L \leq N - 1$, then $q_{s+L} \leq \bar{q}$. Moreover, $q_{s+L+1} < \bar{q}$ and, thus, $q_{s+j} \leq \bar{q}$ for every $N - 1 \geq j \geq L$, since $x_{s+j} \leq \varepsilon_2$ continues to hold. That is, after the first L steps y_n , and hence x_n , begins to increase, as long as $x_n \leq \varepsilon_2$, suggesting that there cannot be infinitely many consecutive indices with $x_n < \varepsilon_2$.

Now let $A = a(1 - b + c)$ and $y_\varepsilon = \log(\varepsilon_2/(1 - \varepsilon_2))$. Then, $y_{n+1} \geq y_n - A$ for all n . Consider a maximal block of consecutive indices starting at $s > 0$ and of length N during which $x_n \leq \varepsilon_2$. First, we have $x_{s-1} > \varepsilon_2$, implying

$y_s \geq y_\varepsilon - A$. Based on the previous discussion, the logits y_n can decrease by at most LA , as after the first L steps, $q_n \leq \bar{q}$ and, so, y_n increases. Therefore, within any such block we have

$$y_n \geq y_\varepsilon - (L + 1)A, \quad n = s, s + 1, \dots, s + N - 1.$$

If there is a block with $s = 0$, then one has $y_n \geq y_0 - LA$. Outside the region $x \leq \varepsilon_2$, we have $y > y_\varepsilon$ and, thus, there exists a constant Y such that $y_n \geq Y$ for all n . Equivalently, there exists $\delta_2 \in (0, 1)$ such that $x_n > \delta_2$ for all n . Combining this result with the upper bound we obtain the claim. \square

Next we show that if $b < cp_0$, then the dynamics induced by (9) is trivial.

Lemma 2. *If $b < cp_0$, then the equilibrium $(0, p_0)$ is globally attracting.*

Proof. Let $q' \in (b/c, p_0)$. Inductively, we have that $q_n - p_0 \geq (1 - k)^n(q_0 - p_0)$. Thus, there exists n_0 such that for all $n \geq n_0$, we have $q_n \geq q'$. Then, for $n \geq n_0$ we have that

$$x_{n+1} \leq \frac{x_n}{x_n + (1 - x_n) \exp(a(x_n - b + q'c))} = h(x_n) < x_n$$

Let $1 > C > e^{-a(q'c - b)}$. There exists an $\eta > 0$ such that $h(x) \leq Cx$ for $x < \eta$. From Lemma 1, there exist a $\delta > 0$ such that $x_n \leq 1 - \delta$ for all n . For $x \in [\eta, 1 - \delta]$, since $h(x) < x$, there exists $\ell_\eta > 0$ such that $h(x) \leq x - \ell_\eta$. If for some $n_1 \geq n_0$ we have $x_{n_1} \in [\eta, 1 - \delta]$, then $x_{n_1+1} \leq h(x_{n_1}) \leq x_{n_1} - \ell_\eta$. As a result, there is an $n_2 \geq n_0$ such that $x_n \in [0, \eta]$ for all $n \geq n_2$. This implies that $x_{n+1} \leq Cx_n$ for all $n \geq n_2$, yielding $\lim x_n = 0$. The convergence of q_n follows. \square

A.2 Connection to the CVaR risk measure

Suppose that the agents evaluate the extreme-event component of action 1 through the Conditional Value-at-Risk measure CVaR_α , at confidence level $\alpha \in (0, 1)$. Then, the perceived cost of action 1, instead of (6), is now given by

$$\tilde{c}_1(x_n, q_n) = N \left(\gamma x_n + M \min \left(1, \frac{q_n}{1 - \alpha} \right) \right).$$

Following the same steps as in the derivation of (9), we arrive at the following system

$$\begin{aligned} x_{n+1} &= \frac{x_n}{x_n + (1 - x_n) \exp \left(a \left(x_n - b + M \min \left(1, \frac{q_n}{1 - \alpha} \right) \right) \right)} \\ q_{n+1} &= (1 - k)q_n + k(p_0 + p_1 x_n), \end{aligned}$$

which governs the dynamics of the agents. We generally assume that $p_0, p_1 \leq 1 - \alpha$, which is natural since they are associated with the extreme-event probabilities. We denote the above map by \tilde{f} , i.e., $(x, q) \mapsto \tilde{f}(x, q)$. In what follows, x_n and q_n refer to the n -th iterate of the system defined by \tilde{f} . The purpose of this Section is to discuss the connections between the dynamics induced by the maps f and \tilde{f} in a semi-analytical manner.

The discussion in Section 2.3 on the equilibria of the system, from both dynamical and game-theoretical perspectives, can be repeated verbatim for the system defined by \tilde{f} . In particular, the content of Lemmas 1 and 2 also holds in this case. For this reason in what follows it is enough to assume that $b > cp_0$. However, the result of Proposition 1 does not directly transfer. In general, one only has that

$$\lim_{n \rightarrow \infty} \frac{1}{n+1} \sum_{i=0}^n \left(x_i + M \min \left(1, \frac{q_i}{1 - \alpha} \right) \right) = b,$$

which is proved by following the same steps as in Proposition 1.

Apart from the similar behavior of the equilibria, the two systems also share deeper connections in terms of their respective dynamics. To this end, we first show the following.

Lemma 3. *We cannot have $q_n > p_0 + p_1$ for all n .*

Proof. Assume the opposite. From Lemma 1, there exists a $\delta > 0$ such that $x_n \leq 1 - \delta$ for all n . Now from the dynamics of q in (9), we have that

$$q_n - (p_0 + p_1) = (1 - k)^n (q_0 - (p_0 + p_1)) - kp_1 \sum_{j=0}^{n-1} (1 - k)^{n-1-j} (1 - x_j)$$

and, as a result,

$$(1-k)^n(q_0 - p_0 - p_1) > kp_1 \sum_{j=0}^{n-1} (1-k)^{n-1-j}(1-x_j) \geq \delta p_1(1 - (1-k)^n).$$

Letting $n \rightarrow \infty$ yields the desired contradiction. \square

Using Lemma 3 and induction, we obtain that $q_n \leq p_0 + p_1$ for all $n \geq n_0$. As a result, if $p_0 + p_1 \leq 1 - \alpha$, then the dynamical phenomena present in the systems defined by f and \tilde{f} coincide. Requiring the condition $p_0 + p_1 \leq 1 - \alpha$ to hold is again natural, recalling the definitions of the parameters p_0 , p_1 , and α . If, however, this condition does not hold, we can still show that for small to moderate values of a , the long-term dynamics of the two systems coincide. To this end, we need first the following lemmas.

Lemma 4. *Suppose $1 - \alpha < p_0 + p_1$ and let $x_c = (1 - \alpha - p_0)/p_1$. Then $x_n > x_c$ cannot hold for all n .*

Proof. Assume the opposite. Let $m(q) = \min(1, q/(1 - \alpha))$. Then, by the dynamics of q we have that

$$q_n \geq (1 - \alpha) - (1 - k)^n p_0 - (1 - k)^n p_1 x_c.$$

As a result, $\lim m(q_n) = 1$. From Lemma 1, there exists a $\delta > 0$ such that $\delta \leq x_n \leq 1 - \delta$ for all n . By the uniform continuity of

$$g(x, m) = \frac{x}{x + (1 - x) \exp(a(x - b + Mm))}$$

on $[\delta, 1 - \delta] \times [0, 1]$ we get that $|e_n| \rightarrow 0$, where we have set $e_n = f(x_n, q_n) - f(x_n, 1 - \alpha)$.

Now we write $h(x) = g(x, 1)$ and $x_{n+1} = h(x_n) + e_n$. Let $1 > C > e^{-a(M-b)}$. Similar to the proof of Lemma 2, there exists an $\eta \in (0, x_c)$ such that $h(x) \leq Cx$ for $x < \eta$ and an $\ell_\eta > 0$ such that $h(x) \leq x - \ell_\eta$ for $x \in [\eta, 1 - \delta]$, where δ is such that $\delta \leq x_n \leq 1 - \delta$ for all n . Let n_0 be such that $|e_n| < \ell_\eta/2$ for $n \geq n_0$. Thus, if for some $n \geq n_0$ we have $x_n \in [\eta, 1 - \delta]$, then $x_{n+1} \leq x_n - \ell_\eta/2$. Therefore, there exists an $n_2 \geq n_0$ such that $x_{n_2} \in [0, \eta]$, yielding a contradiction. \square

Lemma 5. *Suppose $1 - \alpha < p_0 + p_1$ and let $x_c = (1 - \alpha - p_0)/p_1$. If $x_{n_0} \leq x_c$, then $q_n \geq 1 - \alpha$ cannot hold for all n .*

Proof. Assume the opposite. First note that

$$x_{n_0+1} \leq \sup_{0 \leq x \leq x_c} \frac{x}{x + (1 - x) \exp(a(x - b + M))} = \tilde{x} < x_c$$

and so $x_n < x_c$ for all $n > n_0$. Thus, for $n > n_0$ we have

$$q_{n+1} = (1 - k)q_n + k(p_0 + p_1 x_n) < (1 - k)q_n + k(p_0 + p_1 \tilde{x}).$$

As a result, $\limsup q_n \leq p_0 + p_1 \tilde{x} < 1 - \alpha$, contradiction. \square

The next lemma uses Lemmas 4 and 5 to argue that for a up to a certain threshold, the maps f and \tilde{f} induce the same attractors.

Lemma 6. *There exists an a_0 such that for all $a \in (0, a_0)$, $x_0 \in (0, 1)$ and $q_0 > 0$, there exists an n_0 such that $q_n \leq 1 - \alpha$ for all $n \geq n_0$.*

Proof. Let $x_c = (1 - \alpha - p_0)/p_1$ and $q_- = (1 - \alpha)(b - x_c)/M$. Then, under the assumptions on the parameters, we have that $q_- < (1 - \alpha)(1 - x_c) < p_0$. Define

$$a_0 = \max \left\{ a \geq 0 : \max_{0 \leq x \leq x_c} \frac{x}{1 - x} e^{-a(x - x_c)} \leq \frac{x_c}{1 - x_c} \right\},$$

and let $z_n = x_n/(1 - x_n)$. Then,

$$z_{n+1} \leq z_n e^{a(x_c - x_n)}.$$

For $a \leq a_0$, if $x_n \leq x_c$ and $q_n \in [q_-, 1 - \alpha]$, then $q_- < q_{n+1} \leq 1 - \alpha$ and

$$z_{n+1} \leq \frac{x_c}{1 - x_c},$$

from which $x_{n+1} \leq x_c$. As a result, for $a \leq a_0$ the rectangle $[0, x_c] \times [q_-, 1 - \alpha]$ is forward-invariant.

Now notice that since

$$q_{n+1} \geq (1 - k)q_n + kp_0,$$

there exists N_0 such that $q_n \geq q_-$ for all $n \geq N_0$. By Lemma 4, if at some $N_1 \geq N_0$ we have $x_{N_1} \geq x_c$, then there exists $N \geq N_1$ such that $x_N \leq x_c$. If $q_N \leq 1 - \alpha$, then $x_n \leq x_c$ for all $n \geq N$ by the forward-invariance property we showed previously. If $q_N > 1 - \alpha$, then $x_{N+1} < x_N \leq x_c$ since $M > 1 > b$. In any case we conclude that $x_n \leq x_c$ for all $n \geq N$.

Using Lemma 5 and forward-invariance, we get that there exists an $n_0 > N$ such that $q_n < 1 - \alpha$ for all $n \geq n_0$. By the property of forward invariance the result follows. \square

The previous results suggest that, under the natural assumption $1 - \alpha \geq p_0 + p_1$, or, when this condition does not hold, but provided that $a \leq a_0$, the sequence q_n eventually becomes and remains smaller than $1 - \alpha$. Thus, the tail dynamics of the two systems, and consequently their attractors, are identical. For larger values of a , one can numerically verify that the attractors of f and \tilde{f} no longer coincide, but remain qualitatively similar. As an example, consider the parameters $b = 0.9$, $p_0 = 10^{-5}$, $p_1 = 4 \times 10^{-5}$, $k = 0.75$, $M = 1.1$, $1 - \alpha = 3.5 \times 10^{-5}$, $a = 60.2$. For these values, there exist infinitely many indices n for which $q_n > 1 - \alpha$. Both system defined by f and that by \tilde{f} have a unique attractor, which is chaotic, shown in Fig. 16(a) and (b), respectively. The same behavior can be observed for other parameter choices.

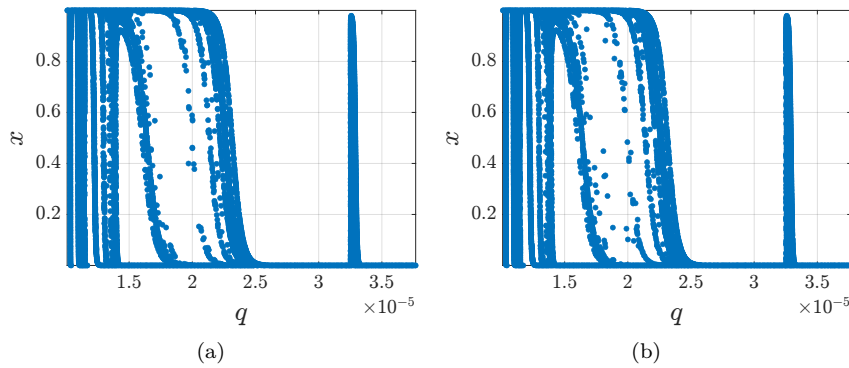


Figure 16: (a) Attractor of the system defined by the map f . (b) Attractor of the system defined by the map \tilde{f} .

References

- [1] Benjamin Allen, Gabor Lippner, Yu-Ting Chen, Babak Fotouhi, Naghmeh Momeni, Shing-Tung Yau, and Martin A Nowak. Evolutionary dynamics on any population structure. *Nature*, 544(7649):227–230, 2017.
- [2] Joaquin Andaluz, A. A. Elsadany, and Gloria Jarne. Dynamic Cournot oligopoly game based on general isoelastic demand. *Nonlinear Dynamics*, 99(2):1053–1063, 2020.
- [3] Gabriel P Andrade, Rafael Frongillo, and Georgios Piliouras. Learning in matrix games can be arbitrarily complex. In *Conference on Learning Theory*, pages 159–185. PMLR, 2021.
- [4] Sanjeev Arora, Elad Hazan, and Satyen Kale. The multiplicative weights update method: a meta-algorithm and applications. *Theory of computing*, 8(1):121–164, 2012.
- [5] James P Bailey, Gauthier Gidel, and Georgios Piliouras. Finite regret and cycles with fixed step-size via alternating gradient descent-ascent. In *Conference on Learning Theory*, pages 391–407. PMLR, 2020.
- [6] James P Bailey and Georgios Piliouras. Multiplicative weights update in zero-sum games. In *Proceedings of the 2018 ACM Conference on Economics and Computation*, pages 321–338, 2018.
- [7] James P Bailey and Georgios Piliouras. Multi-agent learning in network zero-sum games is a hamiltonian system. In *Proceedings of the 18th International Conference on Autonomous Agents and MultiAgent Systems*, pages 233–241, 2019.
- [8] Jakub Bielawski, Thiparat Chotibut, Fryderyk Falniowski, Grzegorz Kosiorowski, Michał Misiurewicz, and Georgios Piliouras. Follow-the-regularized-leader routes to chaos in routing games. In *International Conference on Machine Learning*, pages 925–935. PMLR, 2021.

- [9] Jakub Bielawski, Thiparat Chotibut, Fryderyk Falniowski, Michał Misiurewicz, and Georgios Piliouras. Memory loss can prevent chaos in games dynamics. *Chaos: An Interdisciplinary Journal of Nonlinear Science*, 34(1), 2024.
- [10] Jakub Bielawski, Thiparat Chotibut, Fryderyk Falniowski, Michał Misiurewicz, and Georgios Piliouras. Heterogeneity, reinforcement learning, and chaos in population games. *Proceedings of the National Academy of Sciences*, 122(25):e2319929121, 2025.
- [11] Gian Italo Bischi, Fabio Lamantia, and Bruno Scardamaglia. On the influence of memory on complex dynamics of evolutionary oligopoly models. *Nonlinear Dynamics*, 102(2):1097–1110, 2020.
- [12] Victor Boone and Georgios Piliouras. From Darwin to Poincaré and von Neumann: Recurrence and cycles in evolutionary and algorithmic game theory. In *International Conference on Web and Internet Economics*, pages 85–99. Springer, 2019.
- [13] Tilman Börgers and Rajiv Sarin. Learning through reinforcement and replicator dynamics. *Journal of economic theory*, 77(1):1–14, 1997.
- [14] Colin Camerer and Teck Hua Ho. Experience-weighted attraction learning in normal form games. *Econometrica*, 67(4):827–874, 1999.
- [15] Colin F Camerer, George Loewenstein, and Matthew Rabin. Behavioral economics. *Econometric Society Monographs*, 42:181, 2006.
- [16] Rohitashwa Chattopadhyay, Shubhadeep Sadhukhan, and Sagar Chakraborty. Effect of chaotic agent dynamics on coevolution of cooperation and synchronization. *Chaos: An Interdisciplinary Journal of Nonlinear Science*, 30(11), 2020.
- [17] Yun Kuen Cheung, Stefanos Leonardos, and Georgios Piliouras. Learning in markets: Greed leads to chaos but following the price is right. *arXiv preprint arXiv:2103.08529*, 2021.
- [18] Yun Kuen Cheung and Georgios Piliouras. Vortices instead of equilibria in minmax optimization: Chaos and butterfly effects of online learning in zero-sum games. In *Conference on Learning Theory*, pages 807–834. PMLR, 2019.
- [19] Yun Kuen Cheung and Georgios Piliouras. Chaos, extremism and optimism: Volume analysis of learning in games. *Advances in Neural Information Processing Systems*, 33:9039–9049, 2020.
- [20] Thiparat Chotibut, Fryderyk Falniowski, Michał Misiurewicz, and Georgios Piliouras. The route to chaos in routing games: When is price of anarchy too optimistic? *Advances in Neural Information Processing Systems*, 33:766–777, 2020.
- [21] Thiparat Chotibut, Fryderyk Falniowski, Michał Misiurewicz, and Georgios Piliouras. Family of chaotic maps from game theory. *Dynamical Systems*, 36(1):48–63, 2021.
- [22] George Datseris. DynamicalSystems.jl: A Julia software library for chaos and nonlinear dynamics. *Journal of Open Source Software*, 3(23):598, 2018.
- [23] Alvar Daza, Alexandre Wagemakers, Bertrand Georgeot, David Guéry-Odelin, and Miguel AF Sanjuán. Basin entropy: a new tool to analyze uncertainty in dynamical systems. *Scientific reports*, 6(1):31416, 2016.
- [24] Alvar Daza, Alexandre Wagemakers, and Miguel A.F. Sanjuán. Classifying basins of attraction using the basin entropy. *Chaos, Solitons & Fractals*, 159:112112, 2022.
- [25] A. Dhooge, W. Govaerts, and Yu. A. Kuznetsov. MATCONT: A MATLAB package for numerical bifurcation analysis of ODEs. *ACM Trans. Math. Softw.*, 29(2):141–164, jun 2003.
- [26] Rui Ding, Xianjia Wang, Ji Quan, Shuting Ma, and Jinhua Zhao. Evolutionary dynamics of cooperation in optional public goods games with loners’ punishment. *Chaos: An Interdisciplinary Journal of Nonlinear Science*, 35(3), 2025.
- [27] Maximilian Engel and Georgios Piliouras. A stochastic variant of replicator dynamics in zero-sum games and its invariant measures. *Physica D: Nonlinear Phenomena*, 456:133940, 2023.
- [28] Sinan Feng, Genjiu Xu, Yu Chen, Chaoqian Wang, and Attila Szolnoki. Punishment in bipartite societies. *Chaos: An Interdisciplinary Journal of Nonlinear Science*, 36(2), 2026.
- [29] Yoav Freund and Robert E Schapire. Adaptive game playing using multiplicative weights. *Games and Economic Behavior*, 29(1-2):79–103, 1999.

- [30] Drew Fudenberg and David K Levine. *The theory of learning in games*, volume 2. MIT press, 1998.
- [31] Drew Fudenberg, Martin A Nowak, Christine Taylor, and Loren A Imhof. Evolutionary game dynamics in finite populations with strong selection and weak mutation. *Theoretical population biology*, 70(3):352–363, 2006.
- [32] Tobias Galla and J Doyne Farmer. Complex dynamics in learning complicated games. *Proceedings of the National Academy of Sciences*, 110(4):1232–1236, 2013.
- [33] Celso Grebogi, Edward Ott, and James A. Yorke. Crises, sudden changes in chaotic attractors, and transient chaos. *Physica D: Nonlinear Phenomena*, 7(1):181–200, 1983.
- [34] Christopher Griffin. The replicator dynamics of zero-sum games arise from a novel poisson algebra. *Chaos, Solitons & Fractals*, 153:111508, 2021.
- [35] Christopher Griffin, Riley Mummah, and Russ DeForest. A finite population destroys a traveling wave in spatial replicator dynamics. *Chaos, Solitons & Fractals*, 146:110847, 2021.
- [36] Saeed Hadikhanloo, Rida Laraki, Panayotis Mertikopoulos, and Sylvain Sorin. Learning in nonatomic games, Part I: Finite action spaces and population games. *Journal of Dynamics and Games*, 9(4):433–460, 2022.
- [37] Reza Hakhamanesh, Javad Mohammadzadeh, Hadi Gholami Khaibary, and Masoomeh Azimi. Integrating static and dynamic game theory with complex networks: Enhancing strategy dynamics through adaptive update rules. *Chaos, Solitons & Fractals*, 192:116063, 2025.
- [38] Ralph Hertwig and Ido Erev. The description–experience gap in risky choice. *Trends in cognitive sciences*, 13(12):517–523, 2009.
- [39] Josef Hofbauer and Karl Sigmund. *Evolutionary games and population dynamics*. Cambridge university press, 1998.
- [40] Cars H Hommes. Dynamics of the cobweb model with adaptive expectations and nonlinear supply and demand. *Journal of Economic Behavior & Organization*, 24(3):315–335, 1994.
- [41] Daniel Kahneman and Amos Tversky. Prospect theory: An analysis of decision under risk. In *Handbook of the fundamentals of financial decision making: Part I*, pages 99–127. World Scientific, 2013.
- [42] Michael Kopel. Simple and complex adjustment dynamics in cournot duopoly models. *Chaos, Solitons & Fractals*, 7(12):2031–2048, 1996.
- [43] Walid Krichene, Benjamin Drighes, and Alexandre Bayen. On the convergence of no-regret learning in selfish routing. In *International Conference on Machine Learning*, pages 163–171. PMLR, 2014.
- [44] Madison S Krieger, Sam Sinai, and Martin A Nowak. Turbulent coherent structures and early life below the kolmogorov scale. *Nature communications*, 11(1):2192, 2020.
- [45] Yu. A. Kuznetsov. *Elements of Applied Bifurcation Theory*. Springer Science & Business Media, 3 edition, 2004.
- [46] Cong Li, Tianjiao Feng, Xiudeng Zheng, Sabin Lessard, and Yi Tao. Noise-induced stochastic nash equilibrium in evolutionary game dynamics. *Chaos, Solitons & Fractals*, 192:115970, 2025.
- [47] MingYuan Li, HongWei Kang, XingPing Sun, Yong Shen, and QingYi Chen. Replicator dynamics of public goods game with tax-based punishment. *Chaos, Solitons & Fractals*, 164:112747, 2022.
- [48] Allan J Lichtenberg and Michael A Lieberman. *Regular and chaotic dynamics*. Springer Science & Business Media, 1992.
- [49] Xinle Lin, Jianhe Li, and Suohai Fan. Memory and target payoff enhance cooperation in evolutionary social dilemmas. *Chaos: An Interdisciplinary Journal of Nonlinear Science*, 34(8), 2024.
- [50] Linjie Liu, Xiaojie Chen, and Matjaž Perc. Evolutionary dynamics of cooperation in the public goods game with pool exclusion strategies. *Nonlinear Dynamics*, 97(1):749–766, 2019.
- [51] Ahmed E. Matouk, A. A. Elsadany, and Baogui Xin. Neimark–sacker bifurcation analysis and complex nonlinear dynamics in a heterogeneous quadropoly game with an isoelastic demand function. *Nonlinear Dynamics*, 89(4):2533–2552, 2017.

- [52] Panayotis Mertikopoulos, Christos Papadimitriou, and Georgios Piliouras. Cycles in adversarial regularized learning. In *Proceedings of the twenty-ninth annual ACM-SIAM symposium on discrete algorithms*, pages 2703–2717. SIAM, 2018.
- [53] Brian Mintz and Feng Fu. Evolutionary multi-agent reinforcement learning in group social dilemmas. *Chaos: An Interdisciplinary Journal of Nonlinear Science*, 35(2), 2025.
- [54] Dov Monderer and Lloyd S Shapley. Potential games. *Games and economic behavior*, 14(1):124–143, 1996.
- [55] Archan Mukhopadhyay and Sagar Chakraborty. Deciphering chaos in evolutionary games. *Chaos: An Interdisciplinary Journal of Nonlinear Science*, 30(12), 2020.
- [56] Martin Nowak and Karl Sigmund. Chaos and the evolution of cooperation. *Proceedings of the National Academy of Sciences*, 90(11):5091–5094, 1993.
- [57] Edward Ott. *Chaos in Dynamical Systems*. Cambridge University Press, 2 edition, 2002.
- [58] Gerasimos Palaiopoulos, Ioannis Panageas, and Georgios Piliouras. Multiplicative weights update with constant step-size in congestion games: Convergence, limit cycles and chaos. *Advances in Neural Information Processing Systems*, 30, 2017.
- [59] Varun Pandit, Archan Mukhopadhyay, and Sagar Chakraborty. Weight of fitness deviation governs strict physical chaos in replicator dynamics. *Chaos: An Interdisciplinary Journal of Nonlinear Science*, 28(3), 2018.
- [60] Marco Pangallo, James BT Sanders, Tobias Galla, and J Dooyne Farmer. Towards a taxonomy of learning dynamics in 2×2 games. *Games and Economic Behavior*, 132:1–21, 2022.
- [61] NC Pati. Spiral organization of quasi-periodic shrimp-shaped domains in a discrete predator–prey system. *Chaos: An Interdisciplinary Journal of Nonlinear Science*, 34(8), 2024.
- [62] Ori Plonsky, Peter Ayoub, and Yefim Roth. Underweighting of rare events in strategic games. *Experimental Economics*, pages 1–27, 2025.
- [63] Ori Plonsky and Ido Erev. Learning in settings with partial feedback and the wavy recency effect of rare events. *Cognitive Psychology*, 93:18–43, 2017.
- [64] Drazen Prelec. The probability weighting function. *Econometrica*, pages 497–527, 1998.
- [65] Tõnu Puu. Chaos in duopoly pricing. *Chaos, Solitons & Fractals*, 1(6):573–581, 1991.
- [66] Andreu Puy, Alvar Daza, Alexandre Wagemakers, and Miguel A.F. Sanjuán. A test for fractal boundaries based on the basin entropy. *Communications in Nonlinear Science and Numerical Simulation*, 95:105588, 2021.
- [67] Robert W Rosenthal. A class of games possessing pure-strategy nash equilibria. *International journal of game theory*, 2(1):65–67, 1973.
- [68] James BT Sanders, J Dooyne Farmer, and Tobias Galla. The prevalence of chaotic dynamics in games with many players. *Scientific reports*, 8(1):4902, 2018.
- [69] William H Sandholm. *Population games and evolutionary dynamics*. MIT press, 2010.
- [70] Yuzuru Sato, Eizo Akiyama, and James P Crutchfield. Stability and diversity in collective adaptation. *Physica D: Nonlinear Phenomena*, 210(1-2):21–57, 2005.
- [71] Yuzuru Sato, Eizo Akiyama, and J Dooyne Farmer. Chaos in learning a simple two-person game. *Proceedings of the National Academy of Sciences*, 99(7):4748–4751, 2002.
- [72] Yuzuru Sato and James P Crutchfield. Coupled replicator equations for the dynamics of learning in multiagent systems. *Physical Review E*, 67(1):015206, 2003.
- [73] Colin Sparrow, Sebastian van Strien, and Christopher Harris. Fictitious play in 3×3 games: The transition between periodic and chaotic behaviour. *Games and Economic Behavior*, 63(1):259–291, 2008.
- [74] Ruichen Sun, Hao Zhang, Chengye Zou, Chuan Zhang, and Zhengqi Liu. Attractors and basins of cascading networked evolutionary game under generalized asynchronous update. *Chaos, Solitons & Fractals*, 200:117002, 2025.
- [75] J. M. T. Thompson, H. B. Stewart, and Y. Ueda. Safe, explosive, and dangerous bifurcations in dissipative dynamical systems. *Phys. Rev. E*, 49:1019–1027, Feb 1994.

- [76] Fabio Tramontana and Abd Elalim Abdo Elsadany. Heterogeneous triopoly game with isoelastic demand function. *Nonlinear Dynamics*, 68:187–193, 2012.
- [77] Amos Tversky and Daniel Kahneman. Advances in prospect theory: Cumulative representation of uncertainty. *Journal of Risk and uncertainty*, 5(4):297–323, 1992.
- [78] Sebastian van Strien and Colin Sparrow. Fictitious play in 3×3 games: Chaos and dithering behaviour. *Games and Economic Behavior*, 73(1):262–286, 2011.
- [79] Daniele Vilone, Alberto Robledo, and Angel Sánchez. Chaos and unpredictability in evolutionary dynamics in discrete time. *Physical review letters*, 107(3):038101, 2011.
- [80] Emmanouil-Vasileios Vlatakis-Gkaragkounis, Lampros Flokas, and Georgios Piliouras. Chaos persists in large-scale multi-agent learning despite adaptive learning rates. *arXiv preprint arXiv:2306.01032*, 2023.
- [81] Chao Wang, Tian-jiao Feng, Yan Gao, Yi Tao, and Cong Li. Evolutionary stability in an eco-evolutionary game dynamics with density dependence. *Chaos, Solitons & Fractals*, 168:113141, 2023.
- [82] Yifei Wang, Xinzhu Meng, and Abdullah Khames Alzahrani. Stability, period and chaos of the evolutionary game strategy induced by time-delay and mutation feedback. *Chaos, Solitons & Fractals*, 181:114698, 2024.
- [83] Zhen Wei, Wen Tan, A. A. Elsadany, and Irene Moroz. Complexity and chaos control in a Cournot duopoly model based on bounded rationality and relative profit maximization. *Nonlinear Dynamics*, 111(18):17561–17589, 2023.
- [84] Zhihu Yang and Zhi Li. Oscillation and burst transition of human cooperation. *Nonlinear Dynamics*, 108(4):4599–4610, 2022.
- [85] Hidekazu Yoshioka. An escort replicator dynamic with a continuous action space and its application to resource management. *Chaos, Solitons & Fractals*, 185:114985, 2024.
- [86] Taekho You, Minji Kwon, Hang-Hyun Jo, Woo-Sung Jung, and Seung Ki Baek. Chaos and unpredictability in evolution of cooperation in continuous time. *Physical Review E*, 96(6):062310, 2017.
- [87] Hairui Yuan and Xinzhu Meng. Replicator dynamics of division of labor games with delayed payoffs in infinite populations. *Chaos, Solitons & Fractals*, 158:112058, 2022.